Prediction of aeroelastic response of bridge decks using artificial neural networks

Tajammal Abbas[a,*], Igor Kavrakov[a], Guido Morgenthal[a], Tom Lahmer[b]

[a]*Bauhaus University Weimar, Institute of Structural Engineering, Chair of Modelling and Simulation of Structures, Marienstraße 13A, 99423 Weimar, Germany*
[b]*Bauhaus University Weimar, Institute of Structural Mechanics, Chair of Stochastics and Optimization, Marienstraße 15, 99423 Weimar, Germany*

Abstract

The assessment of wind-induced vibrations is considered vital for the design of long-span bridges. The aim of this research is to develop a methodological framework for robust and efficient prediction strategies for complex aerodynamic phenomena using hybrid models that employ numerical analyses as well as meta-models. Here, an approach to predict motion-induced aerodynamic forces is developed using artificial neural network (ANN). The ANN is implemented in the classical formulation and trained with a comprehensive dataset which is obtained from computational fluid dynamics forced vibration simulations. The input to the ANN is the response time histories of a bridge section, whereas the output is the motion-induced forces. The developed ANN has been tested for training and test data of different cross section geometries which provide promising predictions. The prediction is also performed for an ambient response input with multiple frequencies. Moreover, the trained ANN for aerodynamic forcing is coupled with the structural model to perform fully-coupled fluid–structure interaction analysis to determine the aeroelastic instability limit. The sensitivity of the ANN parameters to the model prediction quality and the efficiency has also been highlighted. The proposed methodology has wide application in the analysis and design of long-span bridges.

Keywords: Artificial neural network; Bridge aerodynamics; Aerodynamic derivatives; Motion-induced forces; Bridges.

1. Introduction

The aeroelastic behaviour of slender structures such as long-span cable-supported bridges is essential to be studied as part of their design as they can develop significant vibrations when exposed to atmospheric wind flow. The trends for increase in the flexibility and reduction of mass of structures make such problems more prominent and the analysis more challenging, thus amplifying the need for accurate, robust and efficient prediction models.

The motion of the structure in the flow induces aerodynamic forces which are characterised by aerodynamic derivatives. These non-dimensional coefficients describe the aerodynamic behaviour of the oscillating deck and are commonly measured through wind tunnel tests (WTT). Aerodynamic derivatives are traditionally used to compute single degree of freedom 'torsional flutter' or coupled two degree of freedom 'classical flutter' [1].

The use of computational fluid dynamics (CFD) simulations has become popular in the last decades to determine aerodynamic forces on a cross section; however, these simulations require significant amount of computational time. The response surface approach is used to reduce the computational effort through representing the complex CFD model by using a simple approximation function. Surrogate modelling can be viewed as a nonlinear inverse problem where the aim is to determine a continuous function of a set of parameters on the basis of limited data. A numerical simulation may take from some minutes to a few days whereas running this approximated function would require only a fraction of this time, thus greatly reducing cost without modifying the existing numerical solver for the simulations [2]. Polynomial regression is commonly used to approximate the model response by polynomial basis functions. Alternatively, the moving least-squares approach [3] has the ability to capture localised regions of the model response. This is achieved by introducing radial weighting functions which depend on the location of the data point being evaluated. The use of surrogate models has been shown to perform efficiently for the sensitivity analysis using the adaptive sampling methods [4–7]. These response surface methods have been used also in the probabilistic torsional flutter [8] and coupled flutter [2, 9] analyses considering structural parameter uncertainties. Moreover, a reduced order model developed by [10] utilizes the impulse response of the cross section obtained from CFD simulations, provides an efficient approach to predict the aerodynamic response of a bridge section. However, the model is unable to capture the nonlinear dynamic behaviour due to linearisation.

*Corresponding author, Tel.: +49 3643 584430
Email address: tajammal.abbas@uni-weimar.de (Tajammal Abbas[a,])

Preprint published in Journal of Computers & Structures 231 (2020) 106198 (https://doi.org/10.1016/j.compstruc.2020.106198)

The use of artificial neural networks (ANN) is relatively new to the field of Wind Engineering. The ANN have been utilized to reproduce partially correlated wind fields [11] and in predicting typhoon design wind speeds and profiles [12]. Jung and Kwon [13] used ANN to predict long-term wind speeds of a site to estimate the annual energy production of wind turbines. Several studies [14–18] have been conducted to employ ANN to predict roof pressure of the structures.

In the last two decades, ANN have started to get some attention to be used in bridge aerodynamics. Some attempts have been made for predicting aerodynamic derivatives of rectangular cross sections [19] and bridge deck sections [20] using ANN. Some more studies on bridge aerodynamics have been done [21, 22] demonstrating the use of ANN framework to model aerodynamic non-linearities in the time domain to capture hysteretic behaviour of aerodynamic systems. Wu [21, 23] predicted the acceleration response for a box section under a turbulent wind flow using ANN trained from WTT data. The aforementioned studies use ANN to predict aerodynamic derivatives or aerodynamic response. However, to the best of authors knowledge, there has been no study which utilizes CFD simulations to develop a meta-model using ANN to predict motion-induced forces.

The aim of this paper is to predict aerodynamic forces on a cross section by reducing the computational effort required by the CFD simulations while maintaining sufficient accuracy. First, a comprehensive database is established for a selected section geometry with its aerodynamic force and response time histories from CFD forced vibration simulations. This dataset is employed as input–output data for the training of an ANN which is later used to predict force time histories for test cases. An advanced strategy to compare time histories is applied to asses the quality of the predicted time histories. The predicted time histories are then used to compute aerodynamic derivatives. This strategy can provide a convenient and feasible option to expand the database to be used for a deck at preliminary design phase. The ANN is also able to predict for a response input with multiple frequencies. Moreover, the ANN meta-model for the aerodynamic forces is coupled with a structural model to calculate flutter limit of the bridge which is also a novel contribution. Further, limit cycle oscillation is predicted, which is a highly nonlinear phenomenon. The developed ANN has been tested for different cross section geometries which provide promising predictions. The large dataset and highly complex nonlinear model behaviour makes ANN an excellent candidate for this purpose. The study shows that the ANN is able to predict aerodynamic behaviour with sufficient accuracy. It allows to compute aerodynamic forces on a section significantly faster than CFD simulations. Since ANN is a data driven approach, it is considered as a 'black box' model [22]. Therefore, the target is not to develop a new model replacing CFD simulations but to make the aerodynamic force prediction process more efficient using advantages of the ANN. The novelty of this approach is that the training of ANN is solely performed through CFD forced vibration simulations. To the best of author's knowledge, this framework has not been presented before. The methodology is equally applicable for the data based on the WTT.

2. Motion-induced aerodynamic forces

The idealisation of a two degrees of freedom system for a section model is shown in Figure 1. The equations of motion can be written as:

$$m\ddot{h} + 2m\xi_h\omega_h\dot{h} + m\omega_h^2 h = F_L, \tag{1a}$$

$$I\ddot{\alpha} + 2I\xi_\alpha\omega_\alpha\dot{\alpha} + I\omega_\alpha^2\alpha = F_M, \tag{1b}$$

where m and I are the mass and mass moment of inertia, ξ_h and ξ_α are the damping ratios, ω_h and ω_α are the natural circular frequencies for the heave and pitch directions, h and α are the vertical displacement and rotation with their first and second time derivatives, F_L and F_M are the lift force and moment, respectively.

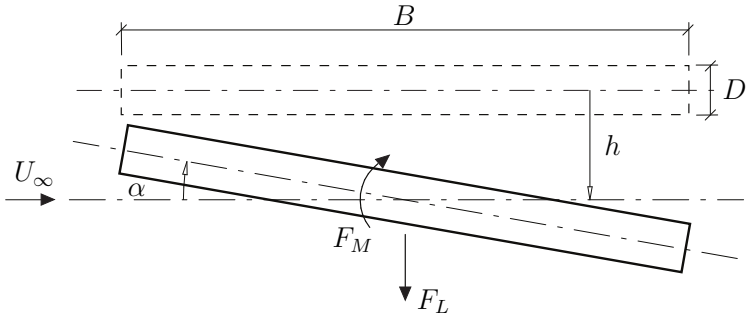

Fig. 1. Definition of degrees of freedom and aerodynamic forces on a cross section.

The motion-induced aerodynamic forces are developed as a result of time dependent motion of the body in a wind flow. These forces produce aerodynamic damping and aerodynamic stiffness into the system. At high wind speeds, negative aerodynamic damping can occur which leads to aeroelastic instability such as flutter. Scanlan and Tomko [24] introduced a mathematical framework for expressing the motion-induced aerodynamic forces on a cross section by aerodynamic derivatives and linear combination of displacements and their first time derivatives. This model has been widely used for the solution of two-dimensional and three-dimensional aeroelastic instability problems in the field of bridge aerodynamics due to its ability to be used for different types of bridge cross sections.

It assumes that the self-excited lift force F_L and moment F_M for a bluff body may be treated as linear in displacement h and rotation α and their first time derivatives [25]. In a linearised form:

$$F_L = \frac{1}{2}\rho U_\infty^2 B\left[KH_1^*\frac{\dot{h}}{U_\infty} + KH_2^*\frac{B\dot{\alpha}}{U_\infty} + K^2H_3^*\alpha + K^2H_4^*\frac{h}{B}\right], \tag{2a}$$

$$F_M = \frac{1}{2}\rho U_\infty^2 B^2\left[KA_1^*\frac{\dot{h}}{U_\infty} + KA_2^*\frac{B\dot{\alpha}}{U_\infty} + K^2A_3^*\alpha + K^2A_4^*\frac{h}{B}\right], \tag{2b}$$

with

$$K = \frac{B\omega}{U_\infty}, \tag{3}$$

where ρ is the air density, U_∞ is the wind speed, B and D are the section width and depth, respectively. H_j^* and A_j^* $(j = 1,\ldots,4)$ are non-dimensional function of K known as aerodynamic derivatives or flutter derivatives which are associated to self-excited lift and moment, respectively. K is the reduced frequency and ω is the frequency of bridge oscillation under aerodynamic forcing. The non-dimensional force coefficients are defined as follows:

$$C_L = \frac{F_L}{\frac{1}{2}\rho U_\infty^2 B}; \qquad C_M = \frac{F_M}{\frac{1}{2}\rho U_\infty^2 B^2}, \tag{4}$$

where C_L and C_M are the lift force coefficient and moment coefficient, respectively. The motion-induced forces are considered to have a linear relationship with the structural motion at relatively small oscillation amplitudes, whereas to take into account nonlinear behaviour, these expressions would include the second-order or even high-order terms of the structural motion.

Theodorsen [26] developed theoretical expressions for unsteady aerodynamic forces acting on a harmonically oscillating flat plate. These forces can also be expressed in terms of equivalent aerodynamic derivatives [25]. This provides the aerodynamic derivatives for a flat plate based on analytical assumptions as follows:

$$H_1^* = -\frac{2\pi}{K}F; \qquad H_2^* = \frac{-\pi}{2K}\left[1 + \frac{4G}{K} + F\right]; \qquad H_3^* = \frac{-\pi}{K^2}\left[2F - \frac{GK}{2}\right]; \qquad H_4^* = \frac{\pi}{2}\left[1 + \frac{4G}{K}\right], \tag{5a}$$

$$A_1^* = \frac{\pi}{2K}F; \qquad A_2^* = \frac{-\pi}{2K^2}\left[\frac{K}{4} - G - \frac{KF}{4}\right]; \qquad A_3^* = \frac{\pi}{2K^2}\left[\frac{K^2}{32} + F - \frac{KG}{4}\right]; \qquad A_4^* = \frac{-\pi}{2K}G, \tag{5b}$$

with

$$C(k) = F(k) + iG(k), \tag{6}$$

where $F(k)$ and $G(k)$ with $k = K/2$ are the real and imaginary parts of Theodorsen's circulation function, respectively. This circulation function is calculated using the Hankel functions and modified Basel functions of first and second kind.

The aerodynamic derivatives are a classical formulation to represent the motion-induced aerodynamic forces and the linear fluid memory effect. As such, they are frequency dependent parameters which are functions of the section geometry, the mean angle of attack, the motion amplitude and the Reynolds number. Since the aerodynamic derivatives are functions of reduced frequency, they can only be measured when the section is in an oscillatory state. The aerodynamic derivatives of a bluff section cannot be computed analytically, since multiple points of separation and reattachment exist on the section boundary which is contrary to the assumption of flat plate theory where there is just a single separation point at the trailing edge. Aerodynamic derivatives can be obtained by performing section model tests in wind tunnels or through CFD simulations. Typically, forced vibration tests are performed under a uniform wind flow.

The classical forced vibration tests are conducted on decoupled motions for simplicity sake. The section is forced to oscillate harmonically in its heave $h = h_o\sin(\omega t)$ or pitch $\alpha = \alpha_o\sin(\omega t)$ degree of freedom with constant peak amplitudes. An empirical relation was suggested in [27] to calculate the peak amplitudes of the vertical and rotational motion for forced oscillation simulations. The detailed procedure to compute aerodynamic derivatives using forced vibration simulation can be found in [28].

Two separate simulations in heave and pitch degree of freedom are required to be performed to get one set of aerodynamic derivatives at a given reduced speed v_r which is defined as

$$v_r = \frac{2\pi U_\infty}{B\omega} = \frac{U_\infty T_o}{B}, \tag{7}$$

where T_o is the period of oscillation.

Since the aerodynamic derivatives are functions of reduced speed v_r, the coupled flutter analysis is traditionally conducted in frequency domain. The flutter analysis requires iterative procedure for the eigenvalue analysis where system frequency and damping ratio are computed at different wind speeds. The nature of eigenvalues describes the stability of the system. The linearised model accounts for the linear memory effects; however, it cannot simulate higher order memory effects, hysteresis phenomenon and limit cycle oscillation [22].

3. Artificial neural network as prediction frame

3.1. Description of a general prediction frame

Machine learning is a powerful technique to obtain a model from a large dataset in order to make predictions. The ANN is one of the forms of machine learning whereby the network is designed to resemble the mechanism of the brain. The brain transmits signals from one neuron to the other. In the same way, the nodes and the arrows in the network represent the data flow (see Figure 2).

The main advantage of the ANN is to express a complex problem using simple mathematical functions. The ANN is significantly efficient as compared to the classical regression approaches, such as polynomial function fitting [29]. , especially when the number of input parameters is large [20]. At the same time, it can efficiently handle multiple outputs.

The prominent features of the ANN are the topology and the learning algorithm. There are several types of ANN based on these features. The essential components of the ANN topology are number of layers, number of neurons in each layer, weights, bias and transfer function. A typical ANN consists of an input layer, one or more hidden layers and an output layer. The network layer contains nodes and every node in a layer is connected to every node in the adjacent layer. Each node in a hidden layer is assigned with a weight and a bias terms.

There are no set rules how the structure of the ANN is to be formed. Usually, it is a trial and error process to find the best configuration depending on the performance and efficiency. This is mainly based on experience and may become a time consuming process. Commonly, a linearly separable function can be well approximated using one hidden layer [30], whereas more than one hidden layers are preferred for practical problems. A multilayer neural network consists of two or more hidden layers. The multilayer neural network has the advantage to capture noisy data and nonlinear behaviour effectively. The multiple layers of the network allow to deal with nonlinear input-output relations that cannot be achieved simply by a single layer at least with the same number of parameters. Such deep networks with much smaller size often show better generalization without significantly increasing the computational complexity.

A neuron in a layer takes the weighted sum of its input neurons and provides the results to its output neuron. The output in the neuron is activated using a transfer function known as the 'activation function'. The activation function can be linear, nonlinear or unity. A commonly used transfer function is 'tanh' which is between -1 and 1 where near the limits it approaches asymptotically.

In a feed-forward network, the information flows from the input layer to the output layer. The input layer collects the data and transmits it to the hidden layer which makes all the computations and provides the data to the output layer. The ANN alters the weights and bias and calculates the error in the output which flows backwards. The error of calculations gets reduced with each iteration where a complete iteration is known as an 'epoch'. Optimization strategies are used in the training process to determine the weights and bias of the nodes for the provided input–output dataset. This is commonly done by steepest-descent algorithm [31]. The step size, which is the length of weight update, is controlled by learning rate. Weight and bias are adjusted to scale the input during the training process to produce the output. Based on the specific learning algorithm, the error in the output is back-propagated to update the weights. The back-propagation of error (BPE) algorithm [32] is commonly used for this purpose because of its simplicity. The training methods are mainly categorized into supervised and unsupervised learning. The former is utilized with back-propagation where the correct output is provided for the training. The latter is used with counter-propagation network which does not require correct output and is used where there is a lack of correct output dataset. The supervised learning is common to be used in both classification and regression applications.

3.2. Multilayer feed-forward neural network

The structure of a multilayer neural network is presented in Figure 2. The ANN serves as a nonlinear meta-model which relates the input X to the output Y as follows:

$$Y = f_{ANN}(X), \tag{8}$$

with

$$X = [x_1, x_2, \ldots, x_P]^{\mathrm{T}}, \tag{9}$$

and

$$Y = [y_1, y_2, \ldots, y_S]^{\mathrm{T}}. \tag{10}$$

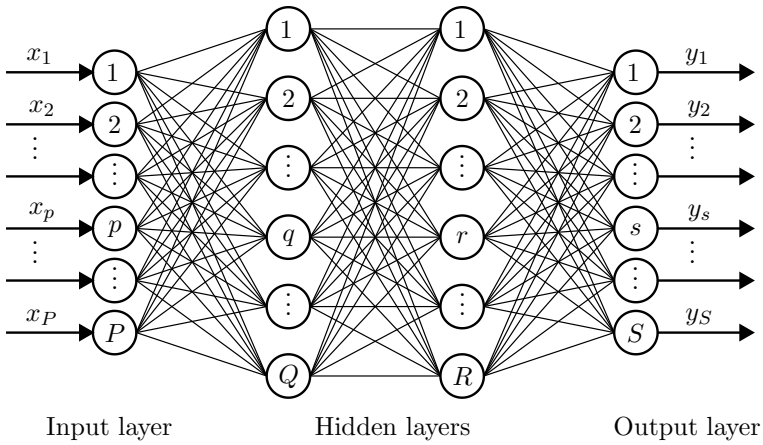

Fig. 2. Schematic of a typical multilayer neural network.

Here, the difference between the training data $\widetilde{Y}$ and the prediction Y of the ANN is needed to be minimized during the training process using an optimization strategy.

The first step of the process is to define an output for each node in the output layer based on the input. The computed output of s^{th} node in the output layer is as follows:

$$y_s = \phi\left(\sum_{r=1}^{R}(w_{rs}u_r + \theta_{rs})\right), \qquad s = 1, 2, \ldots, S \tag{11}$$

with

$$u_r = \phi\left(\sum_{q=1}^{Q}\left(w_{qr}v_q + \theta_{qr}\right)\right), \tag{12}$$

and similarly

$$v_q = \phi\left(\sum_{p=1}^{P}\left(w_{pq}x_p + \theta_{pq}\right)\right), \tag{13}$$

where w_{rs} is the weight between the hidden and the output layer, and w_{pq} is the weight between the input and the hidden layer. θ_{rs} are the bias terms for the output layer and θ_{pq} are the bias for the hidden layer adjacent to the input layer. x_p is the input for the p^{th} node in the input layer. P and S are the number of nodes in the input layer and the output layer, respectively. Q and R are the number of nodes in the hidden layers. Usually, number of nodes in the hidden layers N_H is kept constant i.e. $N_H = Q = R$. The input to each neuron is multiplied with its weight and a bias is added to the weighted sum which is then passed through an activation function to generate the output for that neuron. Thus an output of the ANN becomes a nonlinear function of multiple input parameters. $\phi()$ is the activation function or the transfer function between the computed nodal values and the useful output. The activation function can be linear or nonlinear. A linear transfer function provides output without any change. As a nonlinear transfer function, e.g. the 'tanh' might be applied

$$\phi(a) = \tanh(a) = \frac{2}{1 + e^{-2a}} - 1, \tag{14}$$

where a is the weighted sum including bias as depicted in Eq. (11).

The second step is to calculate the error between the target $\widetilde{Y}$ and calculated Y output. This error is used to monitor the performance of the ANN training process. The weights and bias at each node are calculated and updated by the computed error which is transferred back to the previous nodes using BPE algorithm. The mean squared error (MSE) is calculated as follows:

$$E(g) = \frac{1}{J + S}\sum_{j=1}^{J}\sum_{s=1}^{S}\left(\widetilde{y}_s^j - y_s^j(g)\right)^2, \tag{15}$$

where $\widetilde{y}_s^j$ is the target output value of node s in the output layer for a data point j. J is the total number of output data points. g is the vector of unknown parameters to be determined by optimization and can be written as

$$g = \left[w_{11}, w_{12}, \ldots, w_{pq}, \ldots, w_{PQ}, \ldots, w_{qr}, \ldots, w_{QR}, \ldots, w_{rs}, \ldots, w_{RS}\right]. \tag{16}$$

The final step of the process is to adjust the weights and bias until best performance is achieved which is based on a validation dataset. Here, a hybrid gradient-Newton type descent method is used namely the algorithm of Levenberg-Marquardt [33] which smoothly organizes the transition from steepest-descent search directions towards Newton-search directions, allowing for globally convergent searchers with at least superlinear convergence rates. The error is reduced by using the BPE algorithm to find the optimal values in the training loop as:

$$\Delta w_{pq} = -\eta \frac{\partial E}{\partial w_{pq}}, \tag{17}$$

where η is the learning rate. The Levenberg-Marquardt back propagation algorithm is computationally efficient for moderate size networks. The algorithm is designed without the need to compute the Hessian matrix. The approximated Hessian matrix and the gradient are calculated utilizing the Jacobian matrix. The computation of Jacobian matrix is much simpler than computing the Hessian matrix. However, the Jacobian considers a mean or sum of squared errors E as the performance.

The ANN is first trained using a training dataset before making predictions for a test dataset. The network is trained with an objective to minimize the prediction error. The prediction improves if the network has a better generalization capability. One of the main concerns about the performance of the ANN is to keep a balance between generalization and overfitting. Generalization means that the trained ANN can handle data which has not been used for the training process. When the training is performed repeatedly on the training dataset, after a large number of iterations, overfitting can happen. This implies that the trained ANN will perform significantly well for the training dataset but would fail to perform for the test dataset. This can be avoided by using a validation dataset to have an early stopping. The error for the validation dataset E(validation) is checked at each iteration and at the end of the designated number of epochs, the weights and bias are selected corresponding to the epoch with the least validation error E(validation). Thus, the training dataset is used to change the weights and bias whereas the validation dataset is used as a stopping criterion. After a sufficient training is achieved, the trained network quality is evaluated by its prediction performance and generalization capability for a test dataset which has not been used in the training process. A common observation is that the trained ANN is only able to make accurate predictions for the data range covered by the training dataset whereas predictions outside this range can be erroneous.

4. Prediction frame for motion-induced forces

4.1. Description of the network

The ANN structure described in Section 3.2 has been utilized here for the prediction of motion-induced aerodynamic forces on a cross section. To make efficient and accurate predictions, it is essential to duly define the input and output for the training of the ANN. For this purpose, response and force time histories from the forced vibration simulations are used to train the ANN. Here we use a multilayer, feed-forward, supervised neural network with BPE based on the Levenberg-Marquardt Algorithm. The 'tanh' activation function has been employed for the hidden layers whereas linear activation function is used on the output layer. This algorithm is considered to be the fastest method for training a moderate-sized ANN with up to several hundred weights. The ANN is developed in the MATLAB software environment which contains the network training and optimization algorithms. Additionally, it is easier to reproduce the results, as it is a standardized platform.

As explained in Section 2, the instantaneous motion-induced aerodynamic forces are dependent on the amplitude history of the motion of the oscillating cross section. Therefore, the network presented in Figure 2 has been adopted and modified for this purpose as shown in Figure 3. These figures imply that the lift force coefficient C_L and moment coefficient C_M at any time instance t depend on the history of the motion from time $t-n$ to $t-1$. The response at previous steps is considered to be the input and is associated to the output forces at the current step. The response include displacement, velocity and acceleration whereas output forces are the aerodynamic lift and moment.

For this purpose, Eqs. (9) and (10) are updated accordingly. This is done by replacing x_p $(p = 1, ..., P)$ at the input layer with the response $h(t-i)$ and $\alpha(t-i)$ $(i = 1, .., n)$ and their first and second time derivatives, whereas the output y_s $(s = 1, ..., S)$ at the output layer is replaced with the forces $C_L(t)$ and $C_M(t)$ as

$$\begin{aligned} X = [&h(t-1), \ldots, h(t-n), \dot{h}(t-1), \ldots, \dot{h}(t-n), \ddot{h}(t-1), \ldots, \ddot{h}(t-n), \ldots \\ &\alpha(t-1), \ldots, \alpha(t-n), \dot{\alpha}(t-1), \ldots, \dot{\alpha}(t-n), \ddot{\alpha}(t-1), \ldots, \ddot{\alpha}(t-n)]^{\mathrm{T}}, \end{aligned} \tag{18}$$

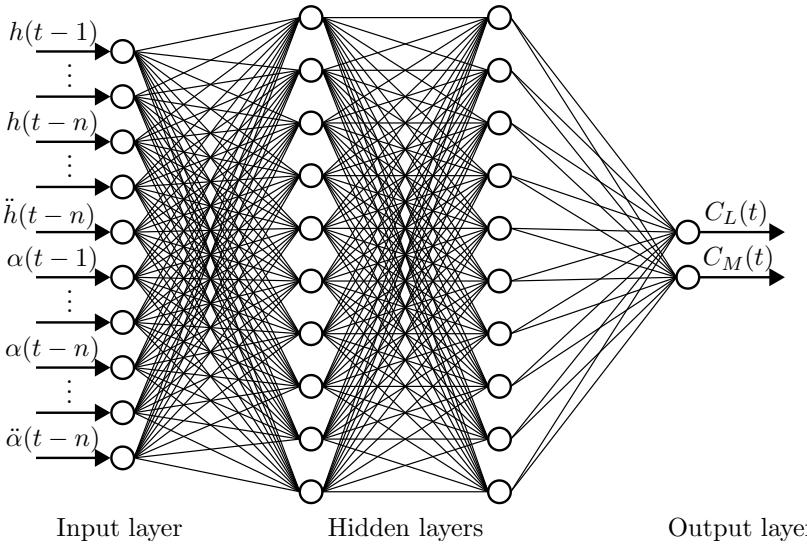

Fig. 3. Schematic of an ANN to predict motion-induced aerodynamic forces on a cross section using response time histories (see Eqs. (8), (18) and (19)).

and

$$Y = [C_L(t), C_M(t)]^{\mathrm{T}} . \tag{19}$$

The training data for the network have been obtained from the forced vibration simulations. The time step Δt in these simulations is kept constant for all reduced speeds v_r. It must be noted that Δt is taken small enough to capture a single period of oscillation with sufficient points at the lowest reduced speed. Whereas, the highest reduced speed is managed by the choice of number of lag terms n to take into account the variation in the response values. This is also necessary as number of lag terms n are related to capturing properly the fluid memory effects. No additional effort was made to find the optimum choice of these parameters for each reduced speed case since the idea was to keep focus on the methodology of the framework.

The reduced speed v_r is not considered in the input to the ANN as later the network is coupled with the structural model for fluid-structure interaction analysis where v_r might be unknown. However, the reduced speed v_r is considered implicitly in the lag terms. In addition to that, wind speed U_∞, section width B and structural natural frequency for heave f_h and pitch f_α are also not considered in the input.

The following sections explain the preparation of the network input data and the training process.

4.2. Preparation of training data

The first step of the training process is to prepare the training data. As depicted in Figure 3, the output of the neural network are the lift force coefficient C_L and moment coefficient C_M at time step t which require the input as response amplitudes h and α with their time derivatives from step $t-n$ to $t-1$. Since in a forced heave simulation the pitch displacements will be zero and vice versa, here both degrees of freedom are considered as input for the network so that a single network structure may be used for both types of simulations. At each time step for the aerodynamic forces as output, the corresponding response values are considered as input. The same process is repeated for all the next time steps. The input and output vectors will have the same number of datasets. The process is repeated for the time histories at all reduced speeds. The generated input for each reduced speed is staked to produce a single input metric with rows as input variables x_P and columns as datasets J. The output metric for each reduced speed is also staked in the same manner.

Since the magnitude of input and output values for each reduced speed case differ greatly, both the input and the output metrics are scaled to have a zero mean and a unit standard deviation for each variable considered. This step is done to avoid any bias introduced due to large magnitude of some variables or to avoid concealing the contribution of other variables with small magnitudes. The normalization factors thus generated are used on the ANN predicted output to scale back to actual units. These normalization factors are also stored and utilized in the preparation of test input data for the ANN prediction.

4.3. Training of artificial neural network

The structure of the network is established by choosing ANN parameters such as number of layers N_L, number of neurons N_H and maximum number of epochs. This will be further elaborated in Section 5. The network training

is performed by using the prepared training data containing input and output metrics. Commonly, the training data are divided into the 'training dataset' and the 'validation dataset' with a ratio of 8 : 2 [34]; however, this ratio is not strictly followed depending on the nature of problem in hand especially when the datasets are large. The training data in this paper are prepared based on simulations with different parameters and therefore this ratio varies. This will be further elaborated in Section 5.

The validation dataset is often chosen at random out of the training data and remaining is treated as the training dataset. However, separate metrics for the training dataset and validation dataset have been created for this study based on selected reduced speeds v_r. This was done to avoid the possibility of choosing data randomly from the time histories corresponding to all v_r ranges considered. Therefore the validation dataset was prepared based on the selected reduced speeds v_r.

During the training process, the error for training dataset E(training) continues to decrease with each epoch. The validation error E(validation) would also decrease; however, at some point it does not decrease further due to over-fitting of the network for the training dataset. When network training stops after reaching the maximum number of designated epochs, the weights and bias corresponding to the lowest validation errors are selected as final or optimum input-output mapping.

4.4. Prediction for test data

The procedure to generate the input data for the test dataset is the same as that of the training data. Since the trained network can only take the same structure of the input for which it has been trained, therefore the test input data has to be prepared in the same manner. Here, the generated input matrix for the test data are scaled using the normalization factors saved during the training data preparation step. The input matrix is then used in the trained network to make predictions and to produce output which also then requires scaling to obtain values in correct units.

The forced oscillation displacements of sinusoidal time histories considered as input are used to predict the motion-induced force time histories which are then used to compute aerodynamic derivatives. For the case of an arbitrary response as input, the network will predict the force time histories accordingly. Such cases are discussed in Section 6.

4.5. Comparison metrics for time histories

Cumulative error measure is used for evaluating the quality of ANN fitting, whereas advance measures are required to compare the target and predicted motion-induced force time histories. Commonly, peak and root mean square (RMS) are calculated which only show a partial comparison for such cases. An advanced approach has been presented by Kavrakov et al. [35] to compare two time histories based on multiple factors which evaluate the time histories using quality measures between 0 and 1. These measures include several comparison metrics; however, for this study the choice is kept limited based on the nature of the problem under discussion. For the sake of brevity, the details of the approach are not discussed in this paper. The considered comparison metrics include: phase $\mathcal{M}_\varphi$, peak $\mathcal{M}_p$, RMS $\mathcal{M}_{rms}$, magnitude $\mathcal{M}_m$ and wavelet $\mathcal{M}_w$. These comparison metrics are developed on exponential basis. A comparison metric equals to 1 indicates that there are no discrepancies in that feature of the time history, while 0 means that the difference is infinite.

$\mathcal{M}_\varphi$ accounts for the mean phase discrepancy between the two signals. It is common but one of the most important parameters in the unsteady aerodynamics that helps to quantify phase shift which is related to the time-lag. The phase between the input motion and the output aerodynamic forces is a typical representation of the fluid memory. The amplitude discrepancy is analysed by $\mathcal{M}_p$ and $\mathcal{M}_{rms}$. These are based on a global and averaged amplitude discrepancies. The peak values of the structural response are considered as essential design criteria. The RMS metric $\mathcal{M}_{rms}$ is determined by the relative difference of the RMS of both signals with respect to the RMS of the reference signal. A relative magnitude metric $\mathcal{M}_m$ is required to investigate the differences of the magnitude in a time-localized manner. By employing the dynamic time warping, the peaks of the signals are aligned and the local phase-shifts and very high frequency components are removed by stretching without scaling. The frequency variation is quantified through wavelet analysis using $\mathcal{M}_w$. This metric helps to investigate the non-stationary behaviour of signals.

5. Verification of accuracy for a flat plate case

Before applying the proposed ANN to the bridge cross sections, the performance of the ANN frame has been tested on an analytical flat plate case. This provides a benchmark solution for the most simplified but a practical scenario.

The flat plate is considered to oscillate harmonically in heave $h = h_o e^{(i\omega t)}$ or pitch $\alpha = \alpha_o e^{(i\omega t)}$ degree of freedom as shown in Figure 4. The generated aerodynamic forces will have the same harmonic frequency ω but a phase shift

of φ [36]. The aerodynamic force from Eq. (2) can be written as follows:

$$C_L e^{i(\omega t-\varphi)} = K^2\left[\left(iH_1^* + H_4^*\right)\frac{h}{B} + \left(iH_2^* + H_3^*\right)\alpha\right]e^{(i\omega t)}, \tag{20a}$$

$$C_M e^{i(\omega t-\varphi)} = K^2\left[\left(iA_1^* + A_4^*\right)\frac{h}{B} + \left(iA_2^* + A_3^*\right)\alpha\right]e^{(i\omega t)}, \tag{20b}$$

where $i = \sqrt{-1}$. C_L and C_M are the non-dimensional lift force and moment, respectively. The aerodynamic derivatives H_i and A_i are obtained from Eq. (5).

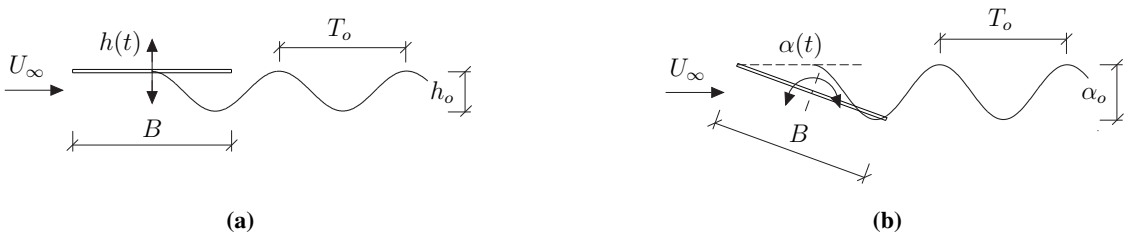

Fig. 4. Schematic of forced vibration motion: **(a)** forced heave motion, **(b)** forced pitch motion.

The time histories of the response and corresponding forces have been generated for particular reduced speeds v_r by using Eq. (20). For this purpose, the oscillation amplitudes $h_o = 0.05B$ for heave and $\alpha_o = 5$ deg for pitch were considered. A constant time step $\Delta t = 0.01$ s was used for all the time histories. A total number of 10,000 steps were considered for each v_r case. The response and force time histories for a flat plate have been prepared at several v_r. It was made sure that for each v_r case, there were atleast 10 cycles of oscillations in order to minimize error originating from the least-squares fit for the determination of aerodynamic derivatives. At the same time, Δt was considered to be small enough to describe each oscillation cycle of a given v_r with atleast 500 time steps. Such a sample time history based on analytical flat plate model can be seen in Figure 7.

This is a relatively simple case with just one peak oscillation amplitude. Since the analytical flat plate model is valid for small amplitudes of oscillation and does not provide dependencies of large amplitudes, only the displacements and rotations have been considered in the ANN input without their time derivatives. The input for the ANN is adapted from Eq. (18) as follows:

$$X = [h(t-1), \ldots, h(t-n), \alpha(t-1), \ldots, \alpha(t-n)]^{\mathrm{T}}. \tag{21}$$

However, the output was considered the same as in Eq. (19). Based on the procedure explained in Section 4, the time history data was prepared for the ANN training.

The selection of suitable parameters is an essential part of the ANN configuration. Therefore, sensitivity of prediction quality to ANN internal parameters has been investigated. The effect of these parameters has been studied only for an analytical flat plate case. The sensitivity study was performed on a limited training data without utilizing the validation data to save computational time. Figure 5 presents the comparison of the quality of training using different ANN parameters. It can be seen that the ANN has a limited capability if less number of neurons N_H or less number of lag terms n are selected. Such models with less ANN parameters show faster convergence and shorter training time due to their simplicity; however, they cannot compete with complex models in terms of quality. For some cases, quality does not improve considerably even though the training time increases proportionally. Since training has to be performed only once, training time is of secondary importance.

The choice of number of hidden layers N_L is commonly associated to the complexity of the problem. This depends on the nonlinearity and generalization requirement of the input data. In case a large number of layers N_L are considered, it may lead to even overfitting which would have high prediction error for the test dataset. The choice of number of neurons N_H in a layer is not only associated to the number of input parameters P but is also to the complexity of the problem. In this paper, equal number of neurons in the hidden layers have been considered (i.e. $N_H = Q = R$). The choice of ANN parameters was made based on achieving the lowest E; however, with reasonable training time. For this case, number of lag terms $n = 5$ were considered. The input layer contains 10 variables which include 5 heave amplitudes and 5 pitch amplitudes at previous time steps. The training data was divided into a training dataset and a validation dataset based on selected reduced speeds. The number of layers $N_L = 3$ and number of neurons in the hidden layer $N_H = 10$ were used. The training was performed until maximum number of specified epochs = 1000 was reached.

For the training dataset, $v_r = 2, 4, 8, 10, 14$ and 16 were considered whereas $v_r = 6$ and 12 were considered for the validation dataset. This division is not based on a specific ratio of the number of training to validation data (see

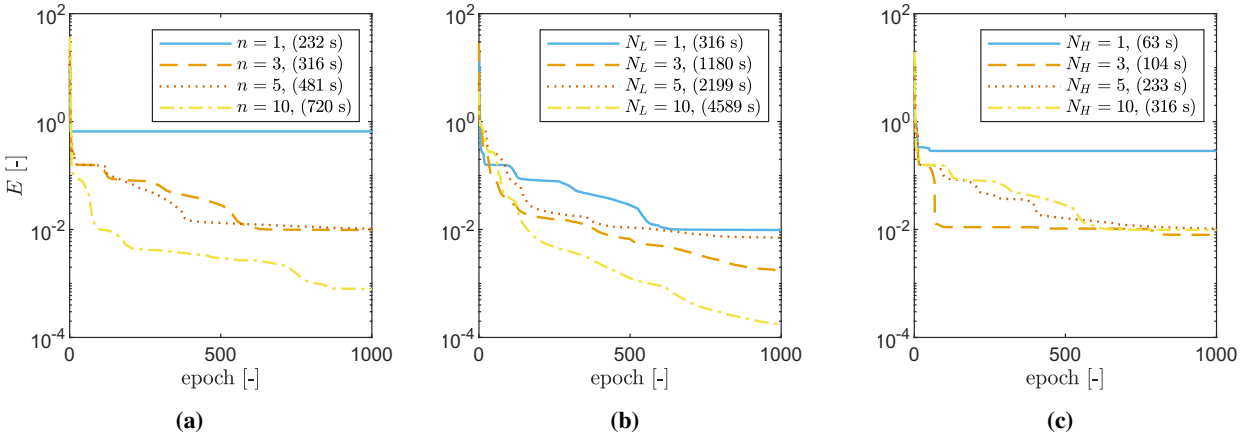

Fig. 5. Flat plate (analytical): sensitivity of ANN parameters to the training performance. Training time is shown in () in legend. Mean squared error E corresponding to different; **(a)** number of lag terms n with $N_L = 1$, $N_H = 10$ **(b)** number of layers N_L with $n = 3$, $N_H = 10$ **(c)** number of neurons in hidden layer N_H with $n = 3$, $N_L = 1$.

Section 4.3), but rather on reduced speeds. This was done to avoid the possibility of randomly choosing training data from the time histories corresponding to all reduced speeds. In that case, the ANN would show overfitting and would not present sufficient generalization for the test data. This consequently generated 158,400 training datasets and 56,400 validation datasets. Figure 6 presents the error in the training process as well as error in the test data. The test data are prepared using $v_r = 1, 3, 5, \ldots, 17, 18, 19$ and 20. It can be seen that the prediction quality is high even outside the training data range for high v_r cases. However, in case of low v_r outside the training data range, the quality is low due to highly nonlinear behaviour at high oscillation frequency. The training time was 1100 s which is not significant considering the size of the data and ANN structure.

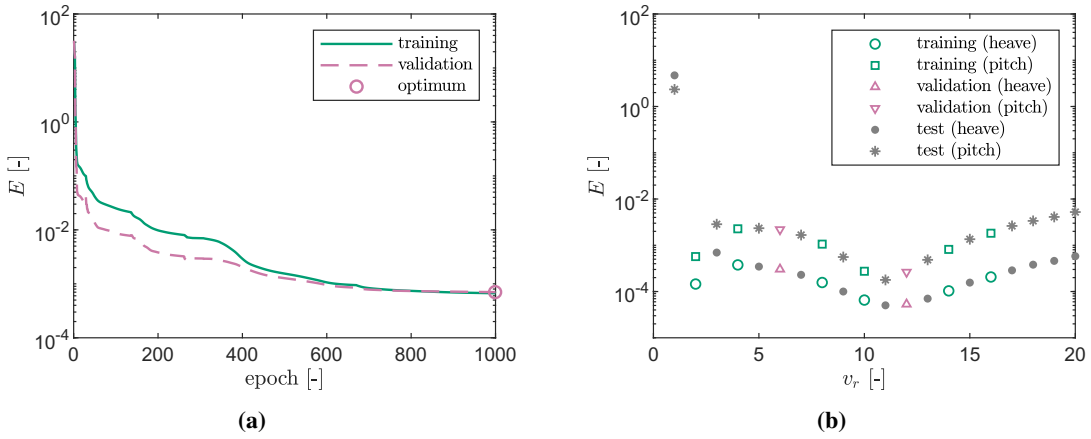

Fig. 6. Flat plate (analytical): performance of ANN training with chosen parameters $n = 5$, $N_L = 3$, $N_H = 10$, training time = 1.25 h; **(a)** mean squared error during training, **(b)** mean squared error for each v_r at the optimum training epoch.

Figure 7 shows a sample force history prediction from the ANN for test data. It shows an excellent agreement with the target. The comparison metric also emphasises the same outcome. Commonly, the comparison metrics are considered good for values above 0.9. The predicted time histories were then used to compute aerodynamic derivatives. Figure 8 depicts the computed aerodynamic derivatives which also shows a good agreement with the analytical values. This comparison indicates that the proposed framework performs really well for the analytical flat plate case. However, some other aspects have not been depicted yet such as noise and dependencies on the amplitude which are associated to the nonlinear behaviour motion-induced aerodynamic forces. Nevertheless, the strategy can be extended as described in Section 6 where these aspects are covered.

6. Prediction frame for CFD simulations

To demonstrate the capability of the proposed framework, the CFD simulation datasets have been used for the considered streamlined and bluff cross sections. Here, two dimensional CFD simulations have been performed in a

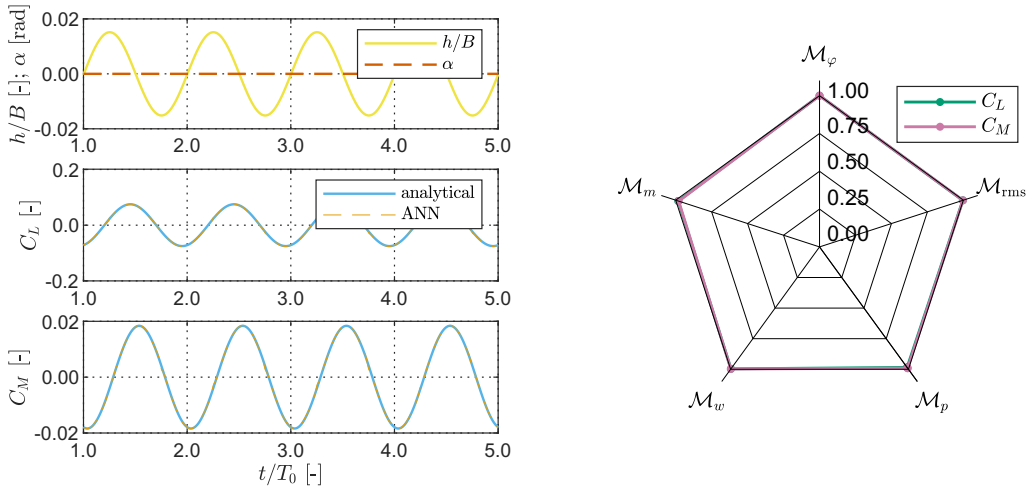

(a) **(b)**

Fig. 7. Flat plate (analytical): sample comparison of force time histories from analytical solution and predictions from ANN for heave case at $v_r = 5$ from test dataset; **(a)** response (displacement h/B and rotation α), lift coefficient C_L and moment coefficient C_M, **(b)** comparison metrics for C_L and C_M.

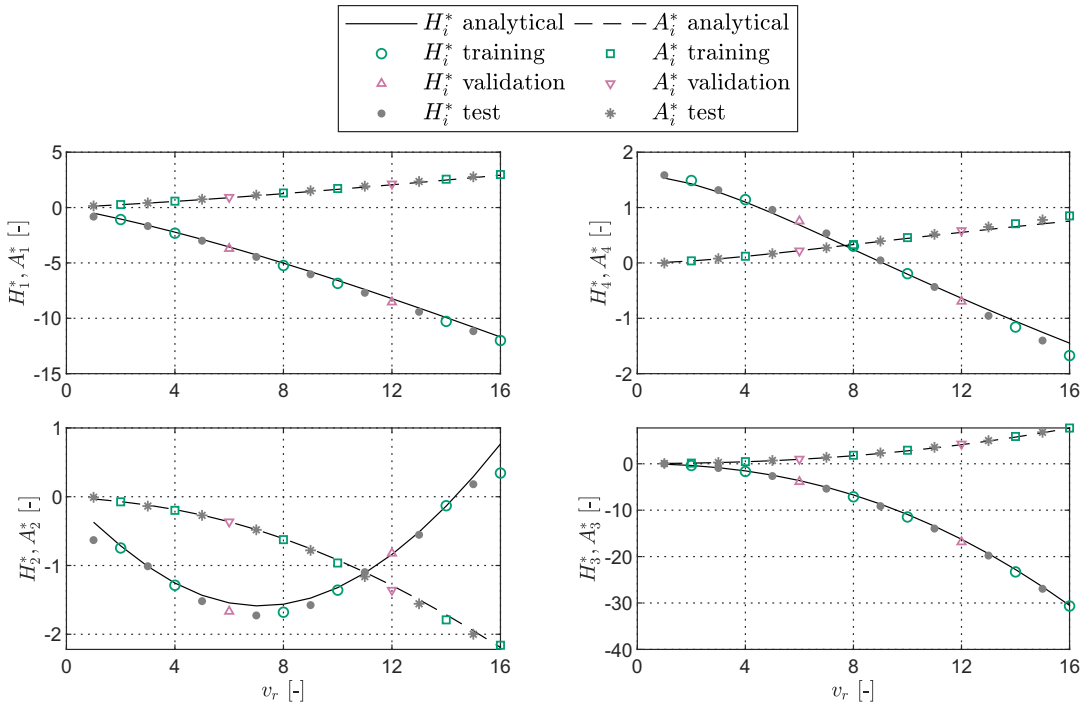

Fig. 8. Flat plate (analytical): comparison of aerodynamic derivatives from analytical solution and computed from force time histories predicted (see also Figure 7) using ANN.

flow solver VXflow based on the vortex particle method [37]. It uses a grid-free Langragian formulation which is computationally efficient as compared to classical Eulerian methods and can be applied to complex structural geometries. Here, Navier-Stokes equations are solved with the help of particles by considering a two dimensional slightly viscous incompressible flow which is suitable for two dimensional bluff bodies. The input to the CFD simulations is the boundary of the bluff cross section, whereas the output are the forces on the section in global degrees of freedom. The boundary of the modelled section is discretised into small panels and the vorticity is discretised on the boundary of the body using the boundary element method. The pressure is computed on the body surface based on the neighbouring velocity and integration of pressure provides forces in the global degrees of freedom. This allows to compute static wind coefficients on the static section whereas aerodynamic derivatives are computed using forced vibration simulations. The vortex-induced vibration response and flutter analysis can be performed using fully-coupled fluid–

structure interaction simulations. For this purpose, the rigid section of the bridge is considered to be suspended on springs which represent its structural dynamic properties. Extensive validation studies on benchmark cases and the real bridge sections have also been performed [28, 38–43]. For the sake of brevity, the details of the aforementioned method have not been presented here.

Forced vibration simulations have been performed to generate the training data for the ANN. For this purpose, the section is forced to oscillate in heave or pitch degree of freedom at a certain reduced speed and aerodynamic forces are determined as described in Section 2. The simulation time was set such that at least 10 cycles of oscillations for each v_r are completed. To have the same Reynolds number for all simulations, the wind speed U_∞ is kept constant. The reduced speed v_r is thus changed by varying the period of the forced oscillation T_o. The response and computed force time histories are then used to generate training data for ANN. The reported data in this paper has been obtained by using a computer with 3.00 GHz Xeon CPU and a 32 GB RAM unless noted otherwise.

Aerodynamic derivatives were also calculated for comparison purposes. The aerodynamic derivatives were computed from the obtained times histories of response and forces using the procedure described in Section 2. Two sets of simulations are performed to produce aerodynamic derivatives corresponding to a certain reduced speed v_r. The time histories and aerodynamic derivatives obtained from the numerical simulations are denoted as 'CFD' whereas predicted using the neural network are denoted as 'ANN'.

6.1. Flat plate case

This section describes development and validation of a suitable ANN model for the motion-induced aerodynamic forces for a flat plate using numerical simulations.

Due to unsteady flow features, such as separation and reattachment, the flow past a cross section produces fluctuating pressures which are integrated at each time step to obtain the section force time histories of lift F_L and moment F_M. These are mainly functions of section geometry, Reynolds number Re and mean angle of attack of wind.

The relevant numerical parameters for this study are given in Table 1. These parameters are identical as the ones used in Kavrakov et al. [44, 45]. For verification of the boundary layer, static wind coefficients and aerodynamic admittance of a static flat plate, further information can be found in the aforementioned study. Figure 9 shows the section of the plate modelled in the CFD solver. The forced vibration simulations have been performed considering the reduced speed v_r upto 16 based on the fundamental frequency of medium to long-span bridges which is commonly within this range. A reduced speed v_r from 2 to 16 was used with a step size of 2. All simulations were run for 20,000 time steps with $\Delta t = 0.00775$ s. The motion-induced forces behave linearly for a small amplitude of oscillations range. To capture the nonlinear behaviour of the motion-induced forces, the simulations have been performed at several peak amplitudes of oscillations h_o and α_o. For this purpose, $h_o/B = 5$ to 45% were considered with a step size of 5%. Similarly, $\alpha_o = 5$ to 45 deg were used again with a step size of 5 deg. Each oscillation amplitude corresponds to 16 sets of time histories of heave and pitch response with lift and moment time histories. A total of 144 simulations were performed. The resulting sample time histories from CFD simulations are presented in Figures 11 and 12.

Fig. 9. Forced vibration simulations on a flat plate (aspect ratio B/D: 200): instantaneous vortex pattern.

Table 1: Flat plate: parameters for CFD simulations.

Item		Value	Unit
Section width	B	31	[m]
Aspect ratio	B/D	200	[-]
Time step	Δt	0.00775	[s]
Reynolds number	Re	10^4	[-]
Wind speed	U_∞	20	[m/s]
Forced vibration simulations		(144 simulations)	
Reduced speed	v_r	2, 4, ..., 16	[-]
Degree of freedom		heave; pitch	
Heave amplitude	h_o/B	5, 10, ..., 45	[%]
Pitch amplitude	α_o	5, 10, ..., 45	[deg]

The data from these simulations have been used for the training of ANN. The training of ANN requires to relate the motion of the oscillating section to its aerodynamic forces. This is done for heave and pitch cases concurrently

in the same manner as described in Section 5. The response and force time histories were then down sampled with a factor of 10 to reduce the amount of data. It is also necessary to limit the number of input parameters for efficiency sake without losing essential information. Here, the input and the output for the ANN are set according to Eqs. (18) and (19).

The same number of lag terms n has been used for the displacement, velocity and acceleration time steps. The input is arranged as described in Section 4. Similarly, the corresponding lift force and moment steps are arranged as output. The process is repeated for each reduced speed of forced vibration simulations. The input to the ANN contains 18 variables and the output contains 2 variables. The input nodes are displacement, velocity and acceleration of the response for heave and pitch with 3 lag terms n each and the output nodes are normalized lift force and moment coefficients.

The training data are divided into the training dataset and the validation dataset. The training dataset includes all the reduced speed values listed in Table 1. However, the validation dataset considers just the reduced speeds v_r from 4 to 16 for all amplitudes of oscillation i.e. 126 simulations. This introduces a bias by not considering a contribution of $v_r = 2$ to avoid a decrease in the quality of training due to highly nonlinear behaviour at this reduced speed.

In addition to the motion-induced forces, the force time histories contain also vortex shedding forces and numerical noise which can be used without any pre-processing or filtering in the training of the ANN. This is the advantage of the ANN that it can handle noisy data effectively. However, some pre-processing is required to be done before using the data for the ANN training. All force and response time histories have been nondimensionalized to obtain values with zero mean and a unit standard deviation.

The ANN training parameters are listed in Table 2. For training, 300 epochs were selected; however, the training was stopped after 144 epochs since there was no considerable improvement noticed as depicted in Figure 10.

Table 2: Flat plate: parameters for ANN training.

Item	Value	Unit	Item	Value	Unit
Number of training datasets	344,236	[-]	n	3	[-]
Number of validation datasets	321,048	[-]	N_L	5	[-]
Number of test datasets	3,800	[-]	N_H	30	[-]
E(training)	1.911	[-]	epoch	144	[-]
E(validation)	0.958	[-]	Training time	50	[h]

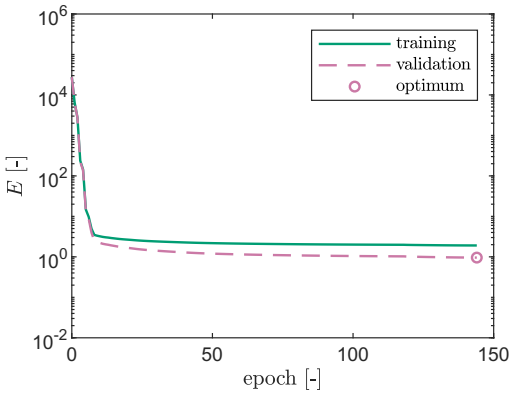

Fig. 10. Flat plate: performance of the ANN training with parameters $n = 3$, $N_L = 5$, $N_H = 30$ with optimum epoch = 144.

After the training the forces have been predicted and the time history comparison is presented in Figures 11 and 12. It can be noted in Figure 11 that at low amplitudes, the motion-induced forces from CFD are linear which is also evident from the fast Fourier transform (FFT) of the forces where a single clear peak at the oscillation frequency is present. However, at large amplitudes, (see Figure 12), multiple contributions from high frequencies are present which indicate the nonlinearity of aerodynamic forces. These plots show that the ANN prediction for forces is really good. It is essential to note that the ANN is not only able to capture the dominant contribution from the motion but also able to capture upto some extent the nonlinearities in the aerodynamic forces at large amplitudes. Although the input to the network is just a harmonic signal with a single frequency, the ANN is able to reproduce a signal with multiple frequencies. This is a significant advantage of using ANN over the classical least-squares fit. Additionally, there is noise in the force time histories which is attributed to the vortex shedding contribution and numerical uncertainty. To overcome this, sufficient number of oscillation cycles or longer length of time history must be considered.

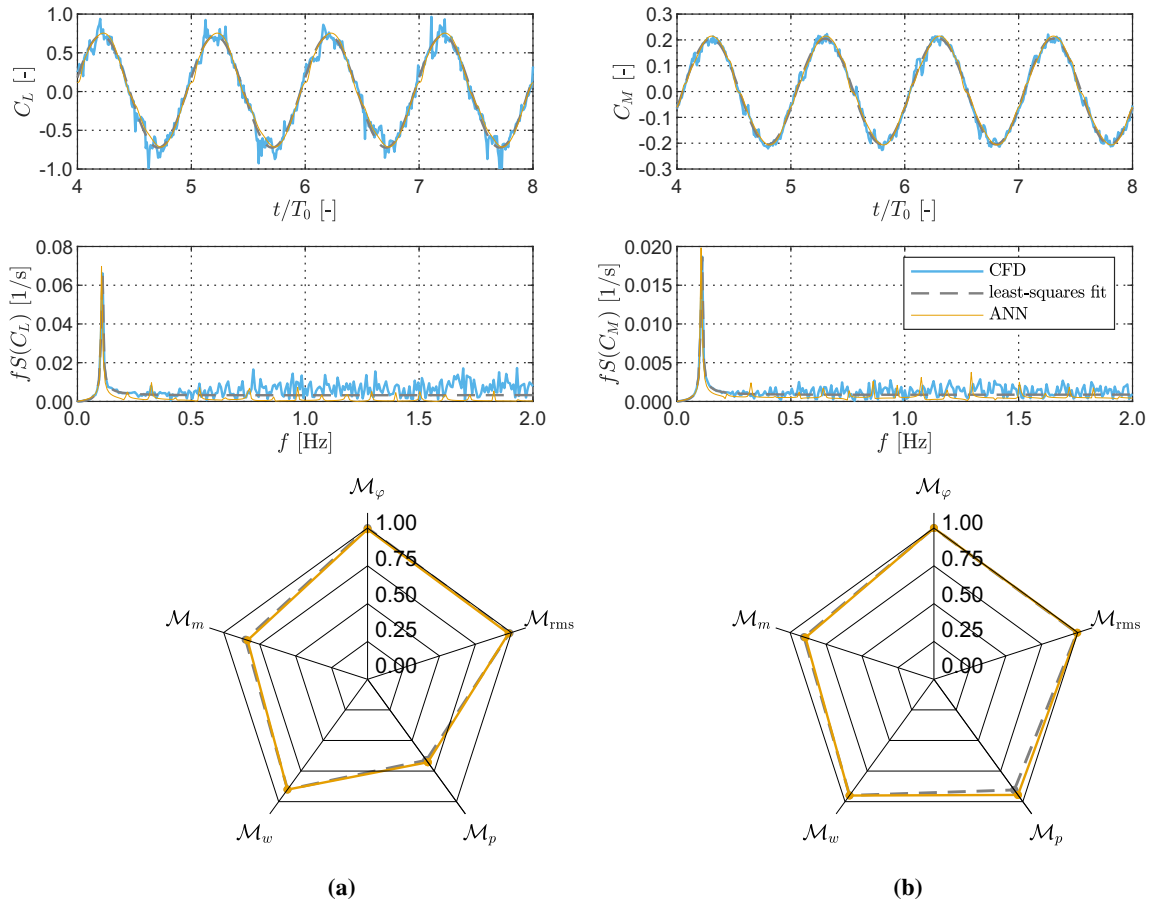

Fig. 11. Flat plate: comparison of force time histories from the CFD simulations and predicted from the ANN for pitch case with $v_r = 6$ at $\alpha_o = 10$ deg; **(a)** time history, spectra and comparison metrics for lift force coefficient, **(b)** time history, spectra and comparison metrics for moment coefficient, (computation time: 67 h for CFD and < 1 s for ANN).

The comparison metrics in Figures 11 and 12 also show the excellent fitting for phase $\mathcal{M}_\varphi$ and RMS $\mathcal{M}_{rms}$ which are the most significant parameters for the current problem. The other components of the comparison metrics also show a good agreement. However, larger differences are found for peak $\mathcal{M}_p$ since vortex shedding forces and numerical noise are included in the force time histories for the case of CFD. Whereas, these effects are filtered in the case of ANN.

Further validation of the approach has been performed by extracting the equivalent sets of time histories from the ANN model and then computing aerodynamic derivatives. To this end, the meta-model is subjected again to standard forced oscillations and the predicted force histories have been used to compute the aerodynamic derivative through standard least-squares fit procedures (see Section 2). Figure 13 illustrates the computed aerodynamic derivatives from the time histories predicted from the ANN. It shows a good agreement with the CFD values. Due to linearised assumption of aerodynamic forces, the aerodynamic derivatives are only computed at lower amplitude range. The figure also provides the flutter limit computed using the aerodynamic derivatives through eigenvalue analysis considering Great Belt Bridge structural properties taken from [27]. The flutter limit is also in good agreement with the CFD ones.

The aerodynamic derivative H_4^* describes the aerodynamic stiffness due to heave motion. The negative value of H_4^* indicate the increase in vertical aerodynamic stiffness and vice versa. On the same lines, A_3^* describes the aerodynamic stiffness due to rotational motion and the positive values implies the decrease of torsional stiffness. Such characteristics of the aerodynamic derivatives lead to the stiffness driven coupled flutter.

The quality of trained network has been evaluated based on the test data which was not used in the training. The forced displacement of linearly increasing oscillation amplitude were considered as shown in Figure 14. This type of response was selected as the test case which shows non-stationarity and resembles a flutter response. The reduced speed $v_r = 8$ was set and the amplitude of oscillation for heave have been gradually increased from 0 to $0.3B$ for over 80 cycles of oscillation. The corresponding lift force and moment time histories were computed as depicted in Figure 14. A good agreement is found for this case.

It is to be noted that the quality of force time history prediction is not the same for the whole v_r range. Additionally, the prediction quality is related to the accuracy of CFD simulations. At large amplitudes, the CFD simulations need

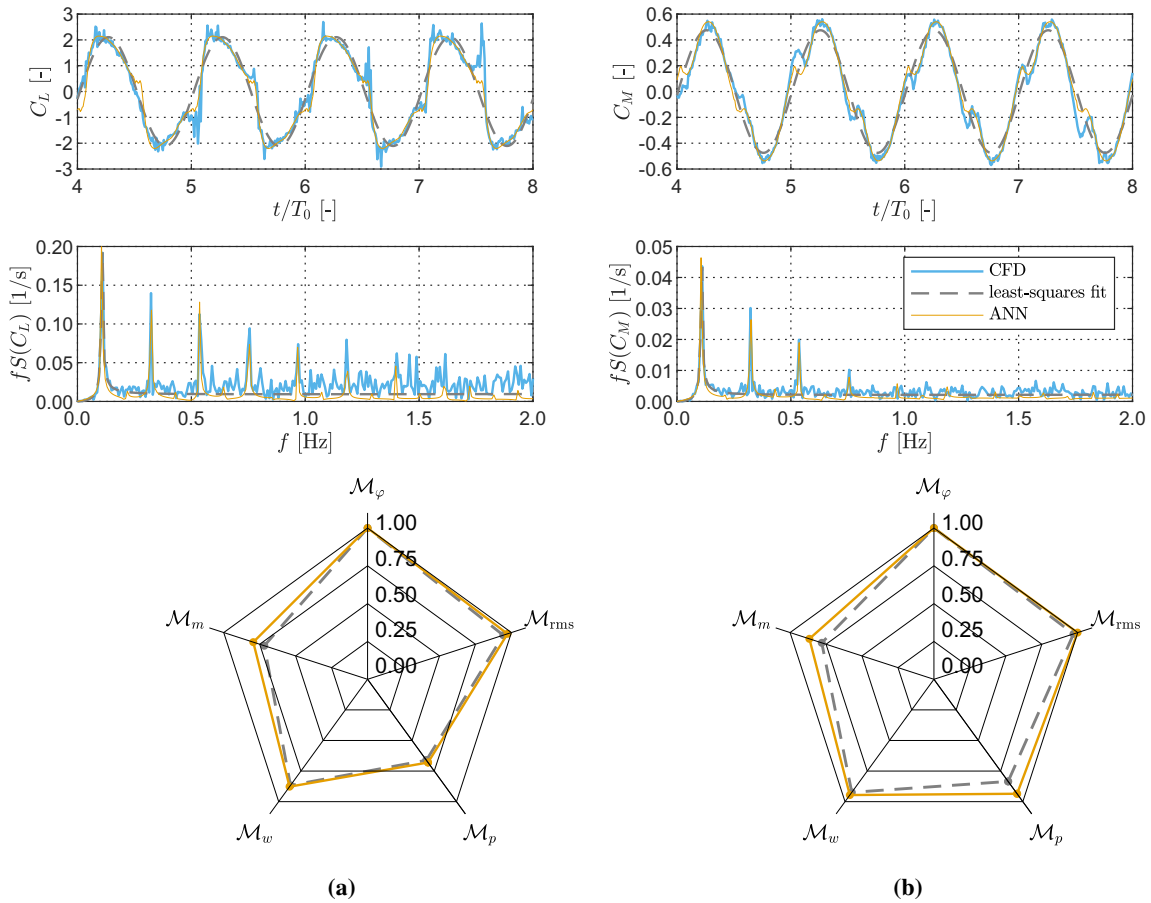

(a) **(b)**

Fig. 12. Flat plate: comparison of force time histories from the CFD simulations and predicted from the ANN for pitch case with $v_r = 6$ at $\alpha_o = 35$ deg; **(a)** time history, spectra and comparison metrics for lift force coefficient, **(b)** time history, spectra and comparison metrics for moment coefficient, (computation time: 28.5 h for CFD and < 1 s for ANN).

sufficiently small time step to resolve flow properly. Since the focus of the paper was not to validate the CFD model, these aspects have not been considered.

Another comparison was made with a random input displacement history with multiple frequencies as presented in Figure 15. The equation of a random forced heave motion containing 3 different frequencies is as follows:

$$h = h_{o,1}\sin(\omega_1 t + \phi_1) + h_{o,2}\sin(\omega_2 t + \phi_2) + h_{o,3}\sin(\omega_3 t + \phi_3), \tag{22}$$

where $h_{o,j} = \{0.2B, 0.15B, 0.10B\}$, $\omega_j = \{0.314, 0.565, 0.754\}$ in rad/s and $\phi_j = \{0, \pi/2.5, \pi/6\}$ in rad with $j = 1, 2, 3$. The motion-induced force prediction was made using the trained ANN and the comparison is shown in Figure 15. The forces from the CFD simulations show the contribution of vortex shedding forces whereas the ANN predictions only present the motion-induced forces. A reasonably good agreement is found indicating that the ANN is able to handle significantly different data effectively. This indicates the generalization capability of the ANN. A significant advantage of the ANN is the unmatched computation time.

6.2. H-shape cross section

The performance of the proposed framework has also been examined for a bluff cross section. For this purpose, H-shape section has been selected which is similar to Tacoma Narrows Bridge cross section. Cables, railing and other attachments have been ignored for the sake of simplicity. The section geometry details are shown in Figure 16. Such cross sections are susceptible to torsional flutter, therefore only the rotational degree of freedom has been considered in this case.

As a first step, CFD forced vibration simulations were performed on the cross section in order to generate the training data. Figure 17 shows the cross section modelled in the flow solver. The parameters presented in Table 3 have been used to carry out CFD simulations in the same manner described in Section 6.1. Here the maximum reduced speed was considered as 8 since the value of A_2^* becomes positive well before 8. This will be further elaborated in this Section. The response and force time histories were also down sampled with a factor of 10.

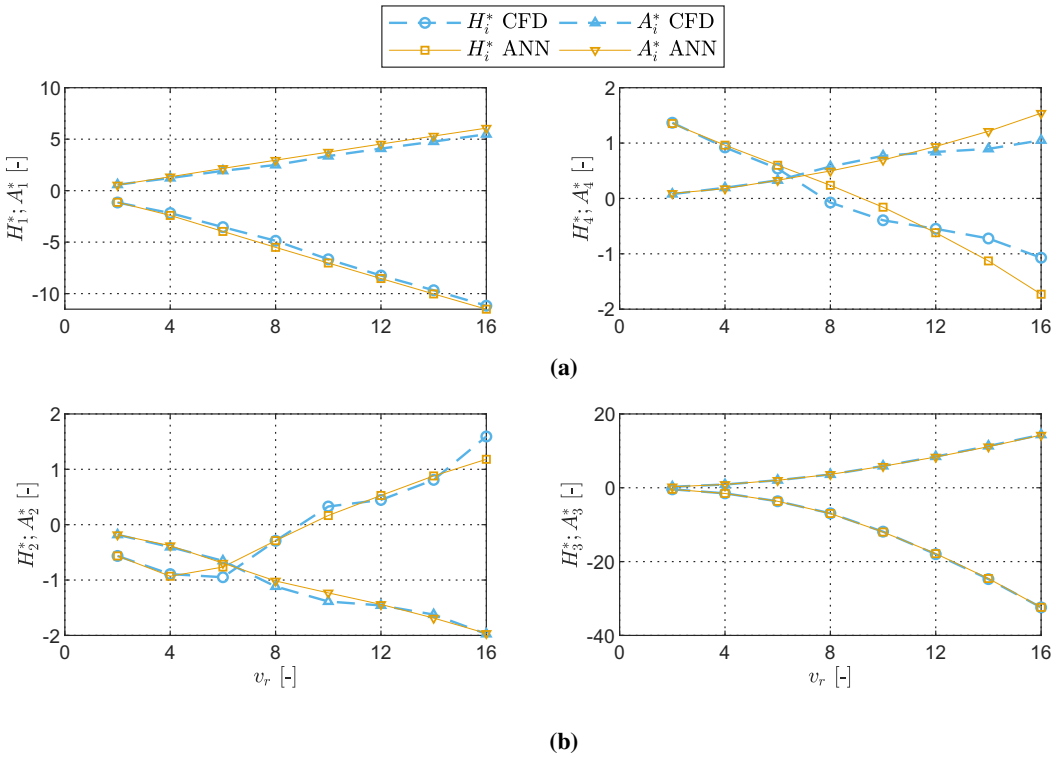

Fig. 13. Flat plate: comparison of aerodynamic derivatives computed from CFD simulations and from force time histories predicted using ANN; **(a)** $h_o/B = 10\%$, **(b)** $\alpha_o = 10$ deg. (see also Tables 1 and 2), (U_{cr}: 66.7 m/s for CFD and 64.6 m/s for ANN).

Table 3: H-shape cross section: parameters for CFD simulations

Item		Value	Unit
Section width	B	12	[m]
Aspect ratio	B/D	5	[-]
Time step	Δt	0.01	[s]
Reynolds number	Re	10^4	[-]
Wind speed	U_∞	10	[m/s]
Forced vibration simulations		(48 simulations)	
Reduced speed	v_r	1, 2, . . . , 8	[-]
Degree of freedom		pitch	
Pitch amplitude	α_o	5, 10, . . . , 30	[deg]

Equal number of lag terms $n = 3$ were considered for the rotational displacement velocity and acceleration. The time histories of response and forces were then used to generate input data for the training process of the ANN as already explained in Section 6.1. For the training dataset $v_r = 1$ to 8 has been selected, whereas for the validation dataset $v_r = 2$ to 6 was chosen. The training was performed using the parameters for the ANN as shown in Table 4.

The input for the ANN is thus adapted from Eq. (18) as follows:

$$X = [\alpha(t-1), \ldots, \alpha(t-n), \dot{\alpha}(t-1), \ldots, \dot{\alpha}(t-n), \ddot{\alpha}(t-1), \ldots, \ddot{\alpha}(t-n))]^{\mathrm{T}} . \tag{23}$$

However, the output was considered the same as in Eq. (19).

Table 4: H-shape cross section: parameters for ANN training.

Item	Value	Unit	Item	Value	Unit
Number of training datasets	82,896	[-]	n	3	[-]
Number of validation datasets	46,075	[-]	N_L	3	[-]
Number of test datasets	7,500	[-]	N_H	50	[-]
E(training)	0.293	[-]	epoch	300	[-]
E(validation)	0.343	[-]	Training time	24	[h]

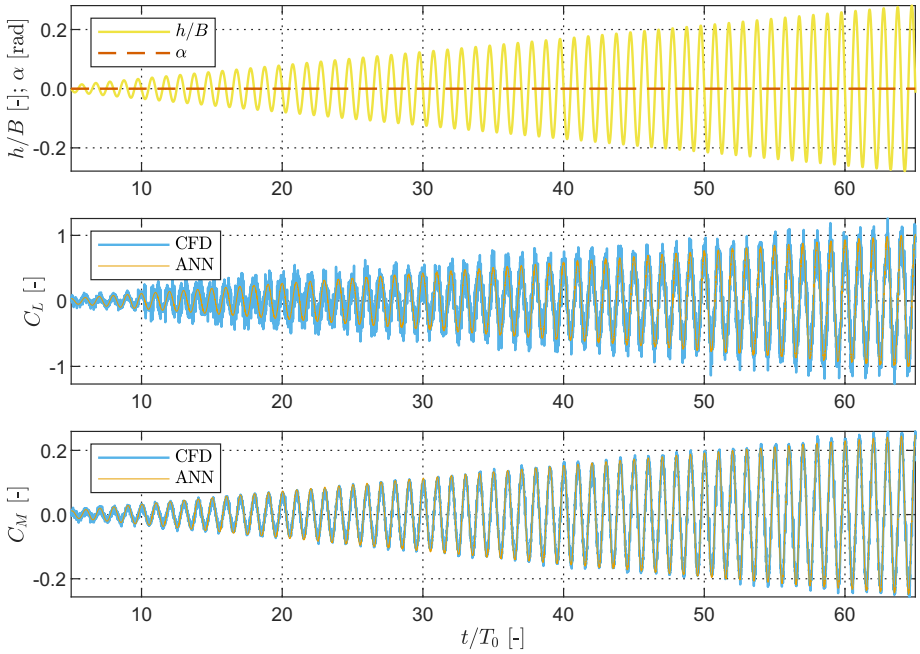

(a)

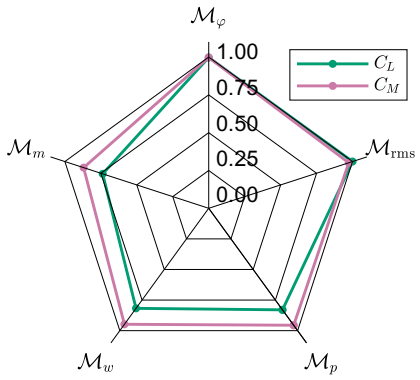

(b)

Fig. 14. Flat plate: comparison of force time histories from the CFD simulations and predicted from the ANN for linearly increasing oscillation response amplitudes from test data at $v_r = 8$; **(a)** response (displacement h/B and rotation α), lift coefficient C_L and moment coefficient C_M, **(b)** comparison metrics, (computation time: 159 h for CFD and < 1 s for ANN).

The training of the ANN was carried out for 300 epochs; however, at epoch = 89, the optimum training was reached as shown in Figure 18.

The performance was first checked for the trained ANN using the data considered in the training. Using the predicted time histories of forces and the corresponding input response, aerodynamic derivatives were computed which are presented in Figure 19. The ANN gives a good prediction for the computed aerodynamic derivatives.

Figure 19 reveals that the value of A_2^* becomes positive at reduced speed $v_r = 5$ indicating the onset of torsional flutter. Such cross sections are susceptible to torsional damping driven flutter behaviour. At higher wind speeds, the net damping of the system which is a combination of structural and aerodynamic damping, becomes positive and the section show flutter response. The aerodynamic derivative A_2^* represents the aerodynamic damping due to rotational motion. The negative value of A_2^* indicate stability which corresponds to the positive aerodynamic damping and vice versa.

In the next step, the trained ANN has been used for the test data which were not used in the training process. To demonstrate this, two cases have been considered. In the first case, the network was subjected to a response time history and the corresponding force time histories were computed. At first, the network was tested on a linearly increasing forced oscillation amplitudes. The simulations in the flow solver were also performed for comparison. A

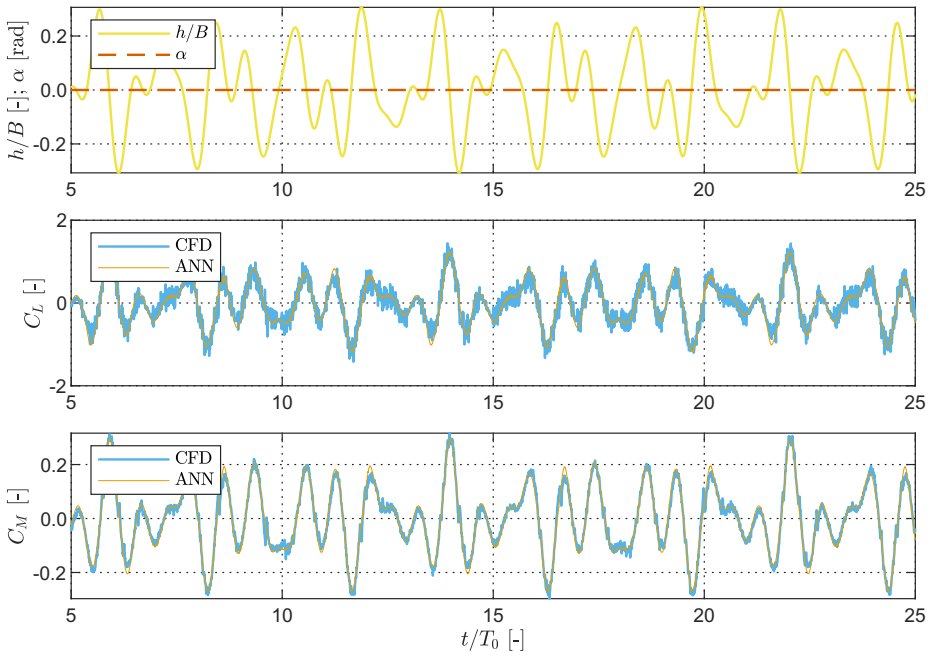

(a)

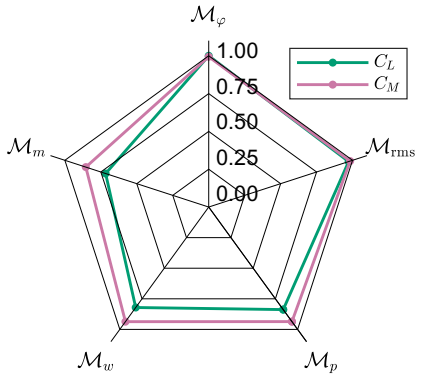

(b)

Fig. 15. Flat plate: comparison of force time histories from the CFD simulations and predicted from the ANN for random response amplitudes for test data, (here $T_o = 2\pi/\omega_2$, see Eq. (22)); **(a)** response (displacement h/B and rotation α), lift coefficient C_L and moment coefficient C_M, **(b)** comparison metrics, (computation time: 39 h for CFD and < 1 s for ANN).

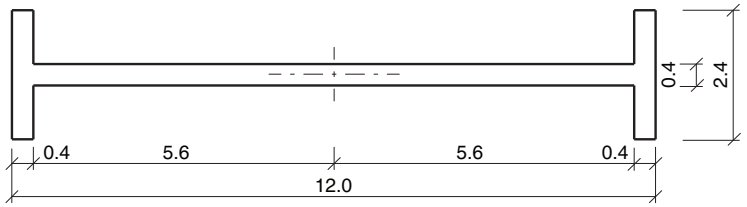

Fig. 16. H-shape cross section details (dimensions in [m]).

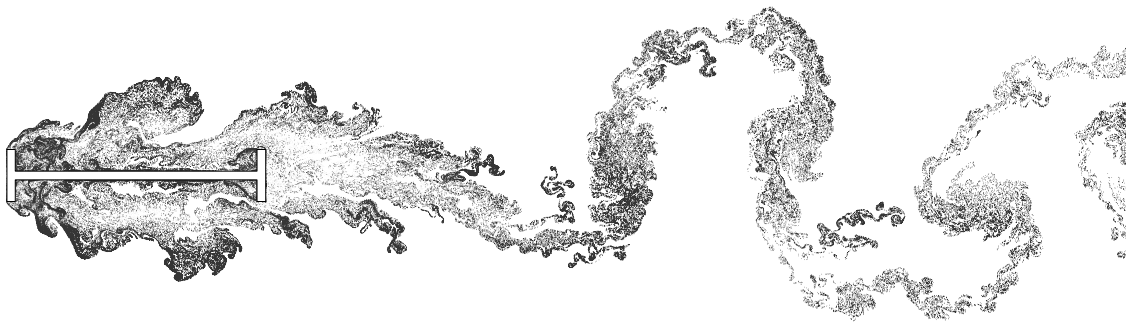

Fig. 17. Forced vibration simulations on H-shape cross section: instantaneous vortex pattern.

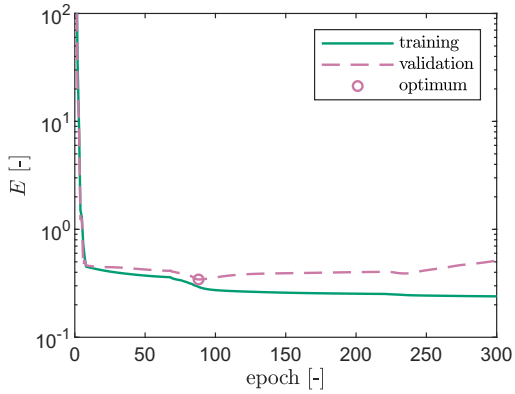

Fig. 18. H-shape cross section: performance of the ANN training with parameters $n = 3$, $N_L = 3$, $N_H = 50$.

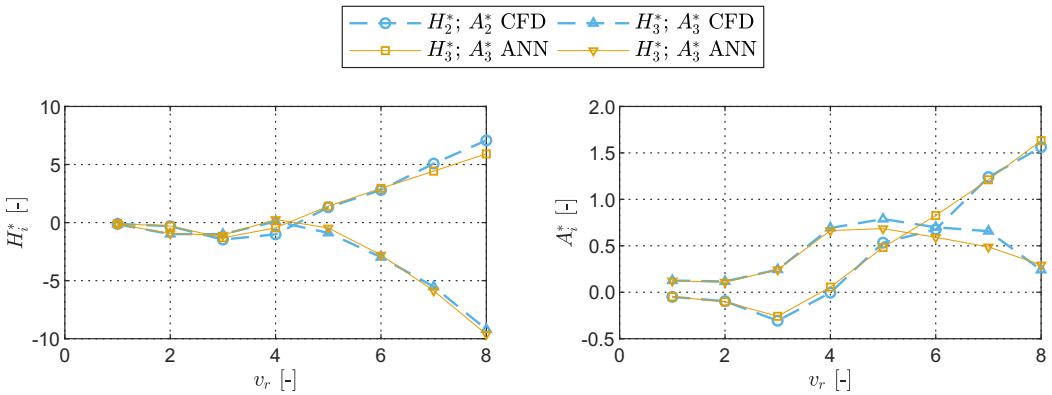

Fig. 19. H-shape cross section: comparison of aerodynamic derivatives computed from CFD simulations and from force time histories predicted from ANN, $\alpha_o = 10$ deg (see also Tables 3 and 4).

reduced speed $v_r = 3$ has been used with a gradually increasing amplitude from 0 to 0.5 rad in about 100 cycles of oscillations. The corresponding lift and moment time histories were determined.

The data were prepared for the ANN input. The prediction for the moment time histories has been made using ANN and is compared in Figure 20. A good agreement is found between the CFD and ANN prediction in general. However, at the start of the time history, discrepancies are observed. This could be associated with two factors. One is the contribution of vortex shedding forces in CFD which is not captured by the ANN and the second is that the training data were not considered at such low amplitude levels. The discrepancies are also captured by the comparison metrics. Although phase and RMS metrics show a good comparison, peak is highly sensitive to noise in the signal. To highlight the non-stationary behaviour in this case, the wavelet coefficients are also plotted. The plot for CFD show noise from high frequencies which is filtered by the ANN.

In the second test case, the ANN prediction quality is evaluated for a fully-coupled CFD simulation by feeding the response at a wind speed above flutter limit. The force time histories are compared in Figure 21. The comparison

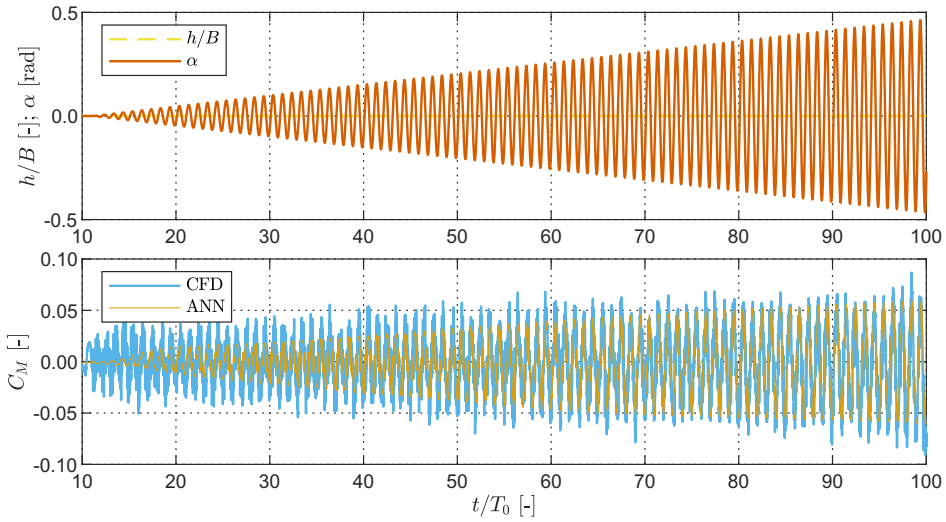

(a)

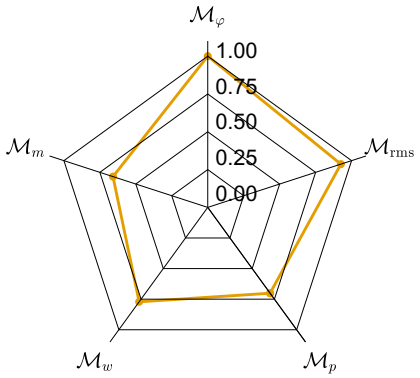

(b)

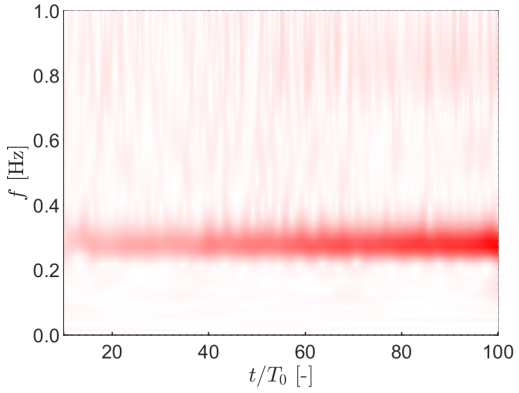

(c)

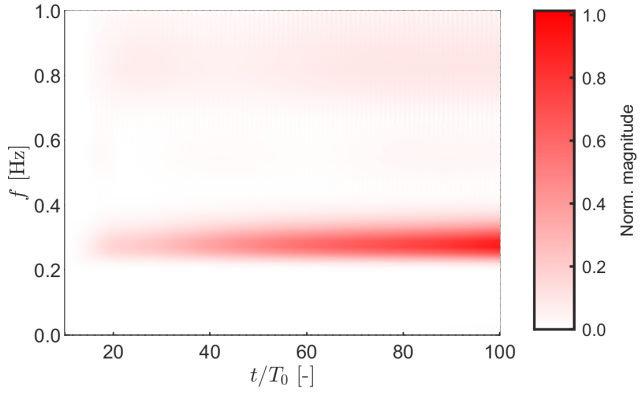

(d)

Fig. 20. H-shape cross section: comparison of force time histories from the CFD simulations and predicted from the ANN for linearly increasing oscillation response amplitudes from test data at $v_r = 3$ (the wavelet coefficients magnitude is normalized with respect to the maximum magnitude of CFD); **(a)** response (displacement h/B and rotation α) and moment coefficient C_M, **(b)** comparison metrics for the moment time history, **(c)** normalized wavelet coefficients for C_M from CFD, **(d)** normalized wavelet coefficients for C_M from ANN, (computation time: 34 h for CFD and < 1 s for ANN).

metrics in general show good quality. The differences are observed in peak and magnitude values which is due to the large contribution of vortex shedding, since the section is bluff in nature. The non-stationary behaviour is evident from the wavelet coefficients along the the time. It also indicates the contribution of high frequencies in the signal from CFD which are smoothed by the ANN.

Additionally, the ANN is coupled with a structural model and the analysis is performed as a fully-coupled fluid–structure interaction problem. For this purpose, the ANN is used as an aerodynamic model and a single degree of freedom structural model is used for coupling. This is done by considering some initial harmonic displacements of the system. Then using these displacements, input for the first time step to the ANN is generated which is then fed into the ANN to predict the forces of the next time step. These forces are then applied to the structural dynamic system and time integration is performed to calculate response corresponding to that step. For this purpose, Newmark time integration scheme [46] was used with average acceleration method. The response obtained at the current and previous steps are once again used to generate the input for the ANN which predicts forces at next step and the whole cycle is repeated in the same manner until the designated time steps are reached.

In this comparison metrics, phase and RMS show accurate prediction by the ANN. The wavelet plots also provide additional information about the non-stationary model behaviour. The CFD wavelet plot indicates contribution of several frequencies in the torsional moment. This is because the CFD model has the additional effect of vortex shedding forces and numerical noise. Whereas the wavelet plot for ANN provides a dominant contribution of only torsional motion frequency. The contribution of excitation frequency is small at the early stage of the time history and gets larger as the amplitudes of oscillation grow. An important point to note is the computational time where ANN beats CFD by a very large extent.

The structural properties of the section include mass moment of inertia, $I = 177.7$ tm^2/m, torsional frequency $f_\alpha = 0.20$ Hz and a damping ratio to critical $\xi_\alpha = 0.01$. The analysis is performed at different wind speeds. The resulting sample time histories are presented in Figure 22. The flutter limit was accurately identified. The model was able to predict divergent response after $U_{cr,ANN} = 10$ m/s which also agrees well to the prediction using fully-coupled CFD simulations i.e. $U_{cr,CFD} = 11$ m/s. It was noted that the prediction of the flutter limit was good when initial amplitudes were considered within the range of the training data. It was observed that the final response amplitudes predicted by the ANN were lower than the corresponding CFD values since motion-induced force contribution alone.

The CFD shows larger force amplitudes, whereas ANN based on the pure sinusoidal input, tries to capture mainly the sinusoidal behaviour of forces and is only able to capture a some contribution of nonlinear effects (see also Figures 11 and 12). The numerical uncertainties and vortex shedding effects have not been considered by the network which are just inherently filtered as noise. The computation time is much larger in this case since at each step input data are prepared, ANN prediction is made and time integration is performed.

7. Conclusions

A framework has been presented to predict aeroelastic response of bridge decks using a hybrid approach by utilizing advantages of CFD and ANN. The ANN are suitable for complex models and can handle significantly large dataset. The proposed ANN framework uses the response and force time histories from the forced vibration tests as the training data. A multilayer feed-forward ANN with Levenberg-Marquardt BPE algorithm has been employed. The trained network is then used to predict motion-induced forces for the test data which shows a good agreement in general; however, the error in the prediction at low reduced speeds in some cases is associated to the highly nonlinear behaviour and numerical uncertainties. The quality of the ANN prediction has been evaluated also by computing aerodynamic derivatives from the predicted motion-induced force time histories which shows reasonably well agreement with the CFD values.

The trained ANN for aerodynamic forcing is coupled with the structural model to perform fully-coupled fluid–structure interaction analysis to determine the aeroelastic instability limit for a bridge section. The successful prediction of the instability limit demonstrates that the ANN framework can be used to predict aeroelastic response of the bridge sections indicating its potential to be applied to other bridge cross sections.

The presented ANN framework provides much more efficient calculations as compared to CFD simulations. It requires a fraction of computational time taken by the CFD simulations. Additionally, the ANN is less sensitive to vortex shedding contribution in the measured force time histories which is treated as noise. The use of noisy data in ANN prevents overfitting of the training data and offers generalization capability of the network. It is found that a reasonable prediction can be made by optimally choosing the ANN parameters.

The paper has shown the advantages of ANN in predicting aeroelastic response. However, the proposed methodology needs sufficient data for proper ANN training before using it for the prediction of motion-induced forces. The quality of CFD simulation itself is an important factor but has not been investigated here. The presented framework is very general and is directly applicable for forces measured in wind tunnel experiments. In such case, the numerical uncertainty that is inherent in the CFD simulations is avoided.

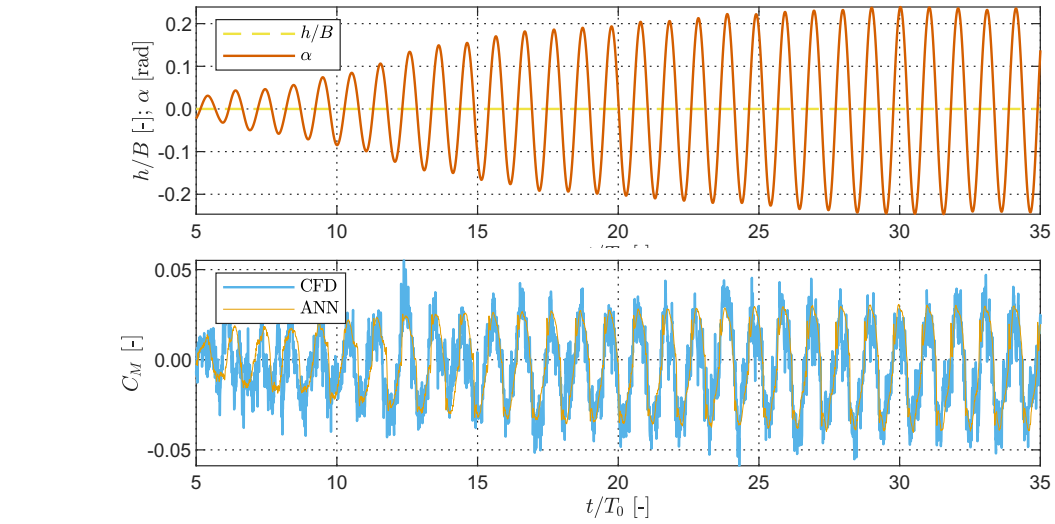

(a)

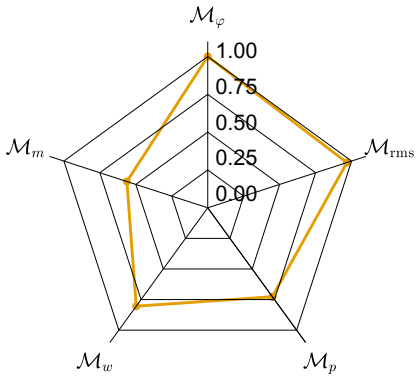

(b)

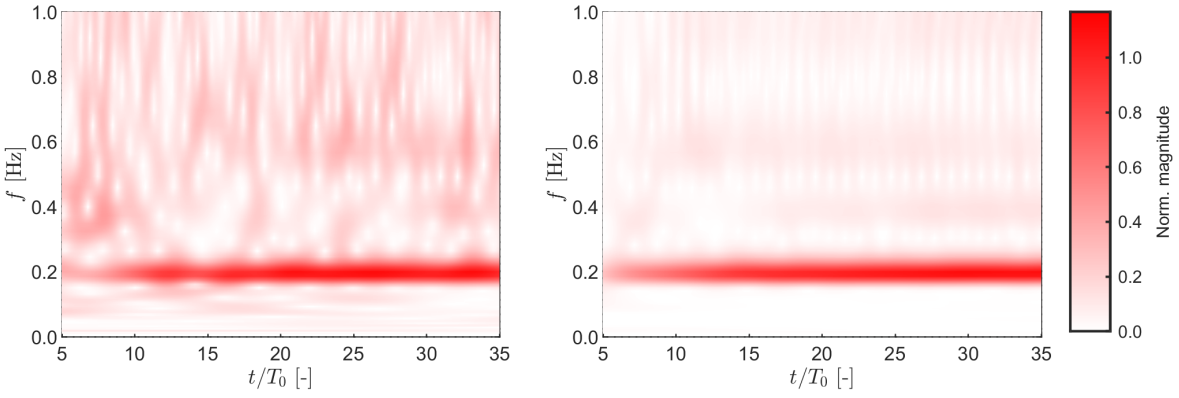

(c) **(d)**

Fig. 21. H-shape cross section: comparison of force time histories from the CFD simulation and predicted from the ANN for a fully-coupled CFD simulations as input to ANN, U_∞=12 m/s (the wavelet coefficients magnitude is normalized with respect to the maximum magnitude of CFD); **(a)** response (displacement h and rotation α) and moment coefficient C_M, **(b)** comparison metrics for the moment time history, **(c)** normalized wavelet coefficients for C_M from CFD, **(d)** normalized wavelet coefficients for C_M from ANN, (computation time: 42.5 h for CFD and < 1 s for ANN).

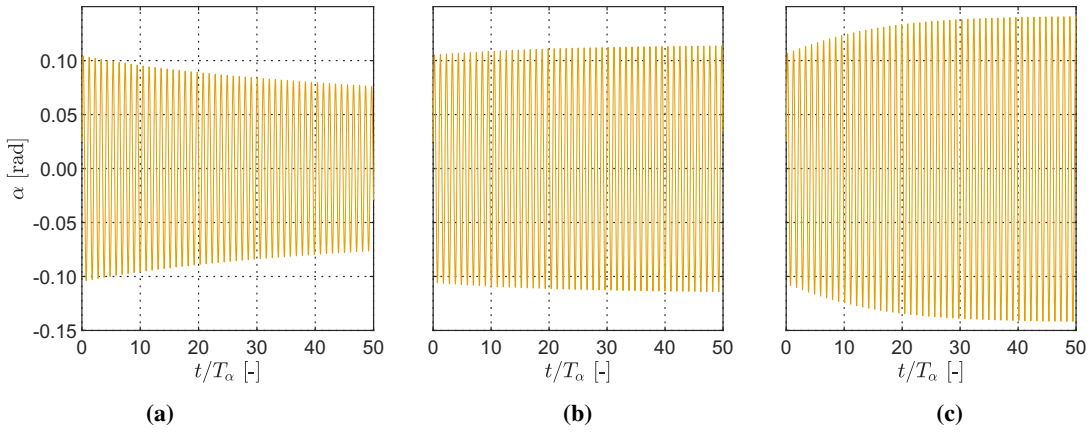

Fig. 22. H-shape cross section: response computed using fully-coupled dynamic fluid–structure interaction analysis using ANN, ($U_{cr,CFD}$ = 11 m/s, $T_\alpha = 1/f_\alpha$); **(a)** U_∞ = 9 m/s, **(b)** U_∞ = 10 m/s, **(c)** U_∞ = 11 m/s, (computation time: 48 h for CFD and 40 s for ANN).

Acknowledgements

This research is supported by the German Research Foundation (DFG) [Project No. 329120866], which is gratefully acknowledged by the authors.

References

References

[1] Abbas, T., Kavrakov, I., and Morgenthal, G. Methods for flutter stability analysis of long-span bridges: A review. *Proceedings of the Institution of Civil Engineers: Bridge Engineering*, pages 1–40, 2017.

[2] Abbas, T. and Morgenthal, G. Framework for sensitivity and uncertainty quantification in the flutter assessment of bridges. *Probabilistic Engineering Mechanics*, 43:91–105, 2016.

[3] Lancaster, P. and Salkauskas, K. Surfaces generated by moving least squares methods. *Mathematics of Computation*, 37(155):141–158, 1981.

[4] Badawy, M. F., Msekh, M. A., Hamdia, K. M., Steiner, M. K., Lahmer, T., and Rabczuk, T. Hybrid nonlinear surrogate models for fracture behavior of polymeric nanocomposites. *Probabilistic Engineering Mechanics*, 50:64–75, 2017.

[5] Steiner, M., Bourinet, J.-M., and Lahmer, T. An adaptive sampling method for global sensitivity analysis based on least-squares support vector regression. *Reliability Engineering and System Safety*, 183:323–340, 2019.

[6] Vu-Bac, N., T.Lahmer, X.Zhuang, T.Nguyen-Thoi, and T.Rabczuk. A software framework for probabilistic sensitivity analysis for computationally expensive models. *Advances in Engineering Software*, 100:19–31, 2016.

[7] Hamdia, K. M., Msekh, M. A., Silani, M., Vu-Ba, N., Zhuang, X., Nguyen-Thoi, T., and Rabczuk, T. Uncertainty quantification of the fracture properties of polymeric nanocomposites based on phase field modeling. *Composite Structures*, 133:1177–90, 2015.

[8] Seo, D.-W. and Caracoglia, L. Estimation of torsional-flutter probability in flexible bridges considering randomness in flutter derivatives. *Engineering Structures*, 33:2284–2296, 2011.

[9] Cheng, J. and Xiao, R. Probabilistic free vibration and flutter analyses of suspension bridges. *Engineering Structures*, 27:1509–1518, 2005.

[10] Ebrahimnejad, L., Janoyan, K. D., Valentine, D. T., and Marzocca, P. Investigation of the aerodynamic analysis of super long-span bridges by using ERA-based reduced-order models. *Journal of Bridge Engineering*, 19(9):1–13, 2014.

[11] Martinez-Vazquez, P. and Rodriguez-Cuevas, N. Wind field reproduction using neural networks and conditional simulation. *Engineering Structures*, 29:1442–1449, 2007.

[12] Huang, W. and Xu, Y. Prediction of typhoon design wind speed and profile over complex terrain. *Structural Engineering and Mechanics*, 45(1):1–18, 2013.

[13] Jung, S. and Kwon, S.-D. Weighted error functions in artificial neural networks for improved wind energy potential estimation. *Applied Energy*, 111:778–790, 2013.

[14] Fernandez-Caban1, P. L., Masters, F. J., and Phillips, B. M. Predicting roof pressures on a low-rise structure from freestream turbulence using artificial neural networks. *Frontiers in Built Environment*, 4(68):1–16, 2018.

[15] Bre, F., Gimenez, J. M., and Fachinotti, V. D. Prediction of wind pressure coefficients on building surfaces using artificial neural networks. *Energy Build*, 158:1429–1441, 2018.

[16] Dongmei, H., Shiqing, H., Xuhui, H., and Xue, Z. Prediction of wind loads on high-rise building using a BP neural network combined with POD. *Journal of Wind Engineering and Industrial Aerodynamics*, 170:1–17, 2017.

[17] Chen, Y., Kopp, G. A., and Surry, D. Prediction of pressure coefficients on roofs of low buildings using artificial neural networks. *Journal of Wind Engineering and Industrial Aerodynamics*, 91:423–441, 2003.

[18] Vrachimi, I., Melo, A. P., and Costola1, D. Prediction of wind pressure coefficients in building energy simulation using machine learning. In *Proceedings of the 15th IBPSA Conference, San Francisco, CA, USA*, 2017.

[19] Chen, C.-H., Wu, J.-C., and Chen, J.-H. Prediction of flutter derivatives by artificial neural networks. *Journal of Wind Engineering and Industrial Aerodynamics*, 96:1925–1937, 2008.

[20] S. Jung, J. G. and Kwon, S.-D. Estimation of aeroelastic parameters of bridge decks using neural networks. *ASCE Journal of Engineering Mechanics*, 130(11):1356–1364, 2004.

[21] Wu, T. and Kareem, A. Modeling hysteretic nonlinear behavior of bridge aerodynamics via cellular automata nested neural network. *Journal of Wing Engineering and Industrial Aerodynamics*, 99:378–388, 2011.
[22] Kareem, A. and Wu, T. Changing dynamic of bridge aerodynamics. *Proceedings of the Institution of Civil Engineers*, 168(SB2):94–106, 2015.
[23] Wu, T., Kareem, A., and Ge, Y. Linear and nonlinear aeroelastic analysis frameworks for cable-supported bridges. *Nonlinear Dynamics*, 74(3):487–516, 2013.
[24] Scanlan, R. H. and Tomko, J. J. Airfoil and bridge deck flutter derivatives. *ASCE Journal of Engineering Mechanics*, 97:1717–1737, 1971.
[25] Simiu, E. and Scanlan, R. H. *Wind Effects on Structures: Fundamentals and Applications to Design*. J. Wiley and Sons, New York, Chichester, Brisbane, 3rd edition, 1996.
[26] Theodorsen, T. General theory of aerodynamic instability and the mechanism of flutter. Report 496, NACA, 1935.
[27] Walther, J. H. *Discrete Vortex Method for Two-dimensional Flow past Bodies of Arbitrary Shape Undergoing Prescribed Rotary and Translational Motion*. Ph.D. Thesis, DTU, Kgs. Lyngby, Denmark, 1994.
[28] Abbas, T. *Assessment of numerical prediction methods for aeroelastic instabilities of bridges*. Ph.D. Thesis, Bauhaus University, Weimar, 2016.
[29] Jaouadi, Z., Abbas, T., and Morgenthal G, L. T. Single and multi-objective shape optimization of streamlined bridge decks. *accepted by Structural and Multidisciplinary Optimization*, 2020.
[30] Cybenko, G. Approximation by superpositions of a sigmoidal function. *Mathematics of Control, Signals, and Systems*, 2:303–314, 1989.
[31] Arfken, G. *Mathematical Methods for Physicists*. 3rd ed. Orlando, FL: Academic Press, 1985.
[32] Hertz, J., Palmer, R. G., and Krogh, A. S. *Introduction to the Theory of Neural Computation*. Perseus Publishing, 1991.
[33] Hagan, M. and Menhaj, M. Training feedforward networks with the Marquardt algorithm. *IEEE Transactions on Neural Networks*, 5(6): 989–993, 1994.
[34] Kim, P. *MATLAB Deep Learning: With Machine Learning, Neural Networks and Artificial Intelligence*. 1st ed. Berkley, United States, 2017.
[35] Kavrakov, I., Kareem, A., and Morgenthal, G. Quantification of the influence of aerodynamic model assumptions for dynamic analyses of bridges. In *40th IABSE Symposium, Tomorrow's Megastructures, Nantes, France*, 2018.
[36] Larsen, A. and Walther, J. H. Discrete Vortex simulation of flow around five generic bridge deck sections. *Journal of Wind Engineering and Industrial Aerodynamics*, 77-78:591–602, 1998.
[37] Morgenthal, G. *Aerodynamic Analysis of Structures Using High-resolution Vortex Particle Methods*. Ph.D. Thesis, University of Cambridge, Cambridge, 2002.
[38] Kavrakov, I. and Morgenthal, G. A synergistic study of a CFD and semi-analytical models for aeroelastic analysis of bridges in turbulent wind conditions. *Journal of Fluids and Structures*, 82:59–85, 2018.
[39] Kavrakov, I. and Morgenthal, G. A comparative assessment of aerodynamic models for buffeting and flutter of long-span bridges. *Engineering*, 3:823–838, 2017.
[40] Kavrakov, I. and Morgenthal, G. Aeroelastic analyses of bridges using a pseudo-3D vortex method and velocity-based synthetic turbulence generation. *Engineering Structures*, 176:825–839, 2018.
[41] Morgenthal, G. and Walther, J. H. An immersed interface method for the vortex-in-cell algorithm. *Computers and Structures*, 85:712–726, 2007.
[42] Sanchez-Corriols, A. and Morgenthal, G. Vortex-induced vibrations on cross sections in tandem arrangement. *Structural Engineering International*, 24:20–26, 2014.
[43] Morgenthal, G. Fluid structure interaction in bluff-body aerodynamics and long-span bridge design: Phenomena and methods. Report CUED/D-STRUCT/TR.187, University of Cambridge, Department of Engineering, 2000.
[44] Kavrakov, I., Argentini, T., Omarini, S., Rocchi, D., and Morgenthal, G. Determination of complex aerodynamic admittance of bridge decks under deterministic gusts using the Vortex Particle Method. *accepted by Journal of Wind Engineering and Industrial Aerodynamics*, 2019.
[45] Kavrakov, I. *Synergistic framework for analysis and model assessment in bridge aerodynamics and aeroelasticity*. Ph.D. Thesis, Bauhaus University, Weimar, 2019.
[46] Chopra, A. *Dynamics of Structures*. Pearson Education, Limited, 2014.